sustainability

MDPI

Article

From Sidewalk Audit to Intervention Priorities: A Transparent, Low-Data Protocol for Sustainable and Inclusive Pedestrian Mobility in Central Blida, Algeria

Lyes Rahmani [1], Abdelmalek Benaradj [2], Radia Bouarroudj [3,*], Soraya Kadri [2], Nassira Messafri [2] and Wided Ratiba Biara [2]

[1] OVAMUS Laboratory (Observatory of the City and Architecture in Urban and Spatial Mutations), Institute of Architecture and Urban Planning, University Saad Dahlab Blida 1, Blida 09000, Algeria; rahmani_lyes@univ-blida.dz
[2] Department of Architecture and Urbanism, University of Tahri Mohamed Bechar, Bechar 08000, Algeria; benaradj.abdelmalek@univ-bechar.dz (A.B.); kadri.soraya@univ-bechar.dz (S.K.); messafri.nassira@univ-bechar.dz (N.M.); biara.wided@univ-bechar.dz (W.R.B.)
[3] Urbanism & Environment Laboratory (LUE), Faculty of Architecture and Urbanism, Salah Boubnider University Constantine 3, Constantine 25000, Algeria
* Correspondence: radia.bouarroudj@univ-constantine3.dz

Abstract

Walking is the most sustainable and socially inclusive urban travel mode, yet in many rapidly transitioning cities, obstructed and inaccessible sidewalks undermine it, and walkability assessment tools rarely tell municipalities where to act first. This study develops a transparent, low-data protocol that converts a micro-scale sidewalk audit into an ordered set of candidate intervention priorities, using 52 street-unit sides nested within 26 street units in central Blida, Algeria. Twenty audit variables were aggregated into eight obstacle families and normalised to occurrences per 100 m using digitised street-unit lengths (170–1255 m). A two-profile *k*-means partition, retained as an operational triage device and stable under street-unit bootstrap resampling, separates lower- and higher-obstruction sides. A random forest with SHAP attribution, validated with folds grouped by street unit, provides an internal ranking of the families that separate the profiles: normative accessibility (27.3%), bulky waste (22.6%), and structural defects (15.9%) lead, with threshold-like effects, and the ordering closely matches simple between-profile contrasts (Spearman ρ = 0.98). Normative accessibility leads under all robustness checks, whereas the order of the second-tier families depends on the number of profiles. Physical works and use regulation carry similar shares of attribution (49.4% and 45.4%); excluding accessibility deficits, which record missing provisions rather than occupied space, shifts the lead clearly to use regulation (62.5%). A minimal agent-based model illustrates how local detours can produce a nonlinear loss of pedestrian performance. The result is a reproducible, low-cost workflow that helps resource-constrained municipalities direct limited budgets towards safe, accessible, and inclusive sidewalks, in line with Sustainable Development Goal 11 (targets 11.2 and 11.7).

Keywords: sustainable urban mobility; inclusive public space; pedestrian accessibility; sidewalk obstruction; intervention prioritisation; micro-scale street audit; decision support; SDG 11; Algeria

Check for updates

Academic Editor: Bo Wang

Received: 10 September 2026
Revised: 17 October 2026
Accepted: 18 October 2026
Published: 4 November 2026

Copyright: © 2026 by the authors. Licensee MDPI, Basel, Switzerland. This article is an open access article distributed under the terms and conditions of the Creative Commons Attribution (CC BY) license.

1. Introduction

Building pedestrian environments that exclude no one has moved from a peripheral design concern to a recognised condition of urban sustainability and spatial justice [1–4]. Although walking is the most universally available travel mode, its practicability depends as much on the micro-scale condition of the sidewalk and on how that sidewalk is managed as on network-level connectivity [5–9]. Two complementary readings of walkability coexist in the literature: one treats it as a measurable property of the built environment, recoverable through systematic audit; the other treats it as an embodied perception that exceeds the physical attributes of space [10–12]. The surfaces on which walking depends are nonetheless seldom audited with the precision applied to carriageways.

Across many rapidly transitioning cities, planning practice has long been organised around the movement of motor vehicles [13,14]. Sidewalks inherit whatever space remains, and that residue is typically discontinuous and encumbered—by structural deficiencies, by poorly managed infrastructure, and by the informal appropriation of public space [15–20].

Blida illustrates the problem acutely: micro-scale auditing reveals sidewalks obstructed to a degree that is simultaneously structural and functional. Two dynamics compound one another—weak coordination between road maintenance and public-works services, and the steady conversion of public space to informal uses such as street trading, unregulated parking, and temporary storage [21–23]. What follows is unequal access, felt first by groups whose mobility is already constrained: young children, older residents, and people with disabilities [24–27]. The study takes its theoretical bearings from Southern urban theory, which holds that analytical categories should be derived from the urban conditions of the Global South rather than imported from elsewhere [28–33]. On this view, cities marked by rapid transition, informality, and the functional saturation of public space are not anomalies to be corrected against an external norm but legitimate sites of theory-building [34–36].

Comparable conditions have been documented in other cities of similar size and street-network density. Studies in North African and Middle Eastern city centres describe car-oriented street design and sidewalks appropriated by vending, parking, and commercial spill-over [37,38], and work in sub-Saharan African cities reports effective sidewalk widths below the minimum needed for two pedestrians to pass, with obstructions forcing pedestrians onto the carriageway [39–41]. These studies point to two lessons relevant here: obstruction rarely has a single cause, and physical improvements need to be paired with the management of how sidewalk space is used [41]. Drawing on these parallels helps to avoid repeating known errors and to transfer tested responses more quickly.

1.1. Research Gaps

The assessment toolkit is by now extensive, yet much of it remains descriptive and static [42–44]. Existing work tends to fall into two broad families: inventories that catalogue barriers and macroscopic analyses built on density, functional mix, and composite indicators of urban form. Recent computer-vision pipelines have substantially improved automated micro-scale measurement from street imagery, but comparatively few studies translate such measurements into transparent, low-data procedures for ranking intervention priorities [45–49]. A second gap concerns the connection between observed obstruction patterns and possible nonlinear changes in pedestrian movement: field audits and behavioural simulation are often developed separately rather than used as complementary diagnostic lenses.

1.2. Research Questions and Objectives

Three questions organise the study. First, among the 20 audited variables, which ones most strongly distinguish lower- and higher-obstruction profiles within the sampled

street units? Second, can a minimal local-avoidance simulation illustrate how increasing obstruction may produce a nonlinear deterioration in pedestrian performance? Third, how do structural failure, fixed street equipment, accessibility deficits, and informal use jointly shape the obstruction burden in central Blida, and what combination of physical works, use regulation, and maintenance is suggested by the observed pattern?

The overarching aim is to develop an exploratory decision-support framework that converts a micro-scale audit into a transparent prioritisation structure for municipal action. The 52 street-unit sides are nested within 26 street units, and this dependence is taken into account in the analysis. Five analytical steps serve this aim: (a) normalising audit counts by street-unit length and partitioning the street-unit sides into obstruction profiles by *k*-means; (b) testing the stability of the profiles by street-unit bootstrap; (c) summarising the profiles with a decision tree and a random forest validated with folds grouped by street unit; (d) ordering obstacle families through SHAP attribution cross-checked against simpler between-profile contrasts; and (e) using a minimal agent-based model to illustrate how local avoidance can generate nonlinear performance loss. The framework is designed for case-based prioritisation and hypothesis generation.

The approach inverts the conventional sequence. Rather than scoring walkability first and diagnosing causes afterwards, it starts from the documented obstacles themselves, describes obstruction profiles from them, and ranks interventions on that basis.

Objective micro-scale audits are an established means of documenting pedestrian barriers in developing countries [37]. This study extends that line of work by linking unsupervised stratification, compact supervised summarisation, and explainable attribution in a single auditable sequence, while checking each elaborate stage against the simpler statistic it might otherwise displace. The contribution is therefore methodological transparency and decision-oriented parsimony rather than algorithmic novelty: the analysis shows both how a low-data audit can be translated into intervention priorities and where more complex modelling ceases to add independent information. The agent-based corridor model is kept separate and is used only to illustrate a possible obstruction mechanism.

The study contributes to urban sustainability in three ways. Environmentally, walking is a zero-emission mode, and keeping sidewalks usable is a precondition for retaining walking trips that would otherwise shift to motorised modes in congested city centres. Socially, the protocol makes accessibility deficits visible and prioritises them, which serves the users whose mobility is most constrained and responds directly to targets 11.2 (accessible transport systems for all) and 11.7 (safe, inclusive, and accessible public spaces) of the 2030 Agenda for Sustainable Development [50]. Institutionally and economically, the protocol requires only a field audit, street-unit lengths and open-source software, so municipalities with limited budgets and data can rank interventions and direct scarce resources where they reduce obstruction most.

2. Materials and Methods

2.1. Study Area and Spatial Sampling

This study investigates the commercial and business centre of Blida, Algeria, through seven structural axes: R1, Rue Cherif Chalabi; R2, Avenue Mustapha Benboulaid; R3, Avenue Al Moukhtar Kritli; R4, Rue Mouhamed Ouali; R6, Boulevard de Mouhamed Boudiaf; R7, Rue Belkacem El Ouazeri; and R8, Avenue Amara Youcef. The axes were selected purposively on two criteria: their structural role as the main streets of the commercial and business centre, and the intensity of commercial activity and pedestrian use along them, which makes interactions between pedestrians and obstacles frequent. Each axis was divided into street units bounded by successive intersections with other surveyed or major streets, giving 26 street units with lengths of 170–1255 m (median 344 m; total

11.6 km). Unit lengths were digitised as centreline polylines in QGIS (WGS 84/UTM zone 31N, EPSG:32631). The right-hand (D) and left-hand (G) sidewalks of each street unit were audited separately, so each street unit contributes two observations, called street-unit sides; the 26 street units therefore yield the 52 street-unit sides analysed. Figure 1 maps the study area and the seven analysed axes.

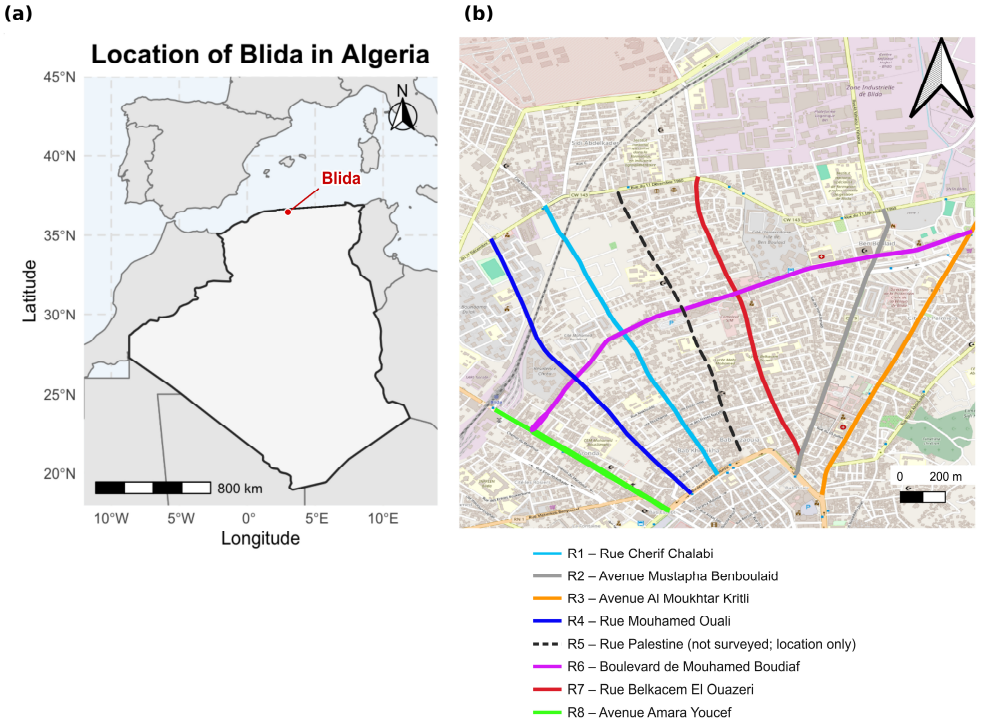


Figure 1. Study area. (**a**) Location of Blida within Algeria; (**b**) the seven surveyed axes within the commercial centre of Blida, labelled in the legend with the codes used in the text (R1–R4 and R6–R8). Rue Palestine (R5), drawn as a dashed dark line, was not audited: it was used only for the observers' preliminary field reconnaissance and is shown for locational context. Base map: © OpenStreetMap contributors (ODbL).

The distribution of street-unit sides is: R1, six; R2, four; R3, eight; R4, six; R6, twelve; R7, ten; and R8, six. Rue Palestine, coded R5 in the survey instrument, was not retained in the audit campaign; the axis is shown in Figure 1 for locational context but contributes no observations. The decision was taken before any analysis and applies to the whole axis, so it cannot have been influenced by the recorded obstruction levels.

Three features of the sampling design bound the analysis. First, the two sides of a street unit share contextual characteristics such as carriageway geometry and commercial frontage; the 52 street-unit sides are therefore nested within 26 street units and are not fully independent, which is addressed by resampling and validating at the street-unit level. Second, street units differ in length by a factor of 7.4, so raw counts confound obstruction intensity with exposure. All counts were therefore converted to occurrences per 100 m of sidewalk before aggregation, partitioning, and attribution; both sides of a street unit are assigned the unit's length. Third, the sample is purposive and concentrated in one central commercial district, so the results describe this district rather than city-wide prevalence. These constraints are revisited in Section 4.5.

2.2. Data Collection and Definition of Audit Variables

A micro-scale inventory of twenty variables was compiled through direct observation. The variables are organised into four thematic categories: (A) infrastructure and

surface deficits—insufficient width (insuff_wid), damaged pavement (damag_coat), excessive cross-slope (exces_bank), and unsuitable curbs/edges (unsuitable_borders); (B) fixed street equipment or elements intersecting the sidewalk—light poles (light_poles), road signs (road_signs), sewer/drainage inlets (mouth_sewer), column bases (column_bases), and street trees (trees), the last of which is aggregated separately as a maintenance family (Table 1); (C) accessibility-compliance deficits—absence of tactile paving (tactile_bands) and access ramps (access_ramps); and (D) temporary, commercial, and management-related obstructions—market stalls (march_shops), merchandise on the sidewalk (merchandise), advertising panels (advertising_panels), unauthorised parking (anarchic_park), waste/garbage (waste_garbage), bulky items (bulky_items), loose rubbish (rubbish), debris (debris), and construction works (work). All variable codes are written in lowercase.

Table 1. Aggregation rules for synthetic variables X1–X8. Each synthetic score is the sum of the occurrences per 100 m of its constituent audit variables for a street-unit side; the scores are relative burden indicators rather than calibrated physical units.

Synthetic Variable	Calculation/Components
X1 Structural defects	insuff_wid + damag_coat + exces_bank + unsuitable_borders
X2 Street furniture	light_poles + road_signs + column_bases + mouth_sewer
X3 Normative accessibility	tactile_bands + access_ramps (recorded as missing accessibility provisions)
X4 Commercial occupation	march_shops + merchandise + advertising_panels
X5 Illegal parking	anarchic_park
X6 Bulky waste	waste_garbage + bulky_items + debris + rubbish
X7 Natural obstacles	Trees
X8 Construction sites	Work

The variables are encoded as counts of recorded obstacle or deficit occurrences on the audited side of each street unit. An occurrence is therefore an audit-score unit and does not necessarily represent an object of identical physical size or severity across variables; this distinction is particularly important for width, surface-condition, and accessibility deficits. The counting unit differs in kind between present and absent features. For a present obstacle, one occurrence is one discrete object intersecting the clear pedestrian path. For the two accessibility-deficit variables (tactile_bands, access_ramps), an occurrence is a location at which the provision is required by Law No. 02-09 but is absent, enumerated over the extent of the street-unit side. This makes X3 different in kind from the object-count families: it counts required-but-missing provisions rather than physical objects occupying the walking surface, and its magnitude therefore grows with the number of compliance points a street-unit side contains. Section 4.4 reports a sensitivity analysis in which X3 is removed from the attribution, and Section 4.5 states the consequences for interpretation. The audit protocol and its quality control are described below; their implications for reliability are discussed in Section 4.5.

Data collection was carried out during the 2024/2025 academic year by 25 third-year students of the Institute of Architecture and Urban Planning, University Saad Dahlab Blida 1, working in seven teams of three to four students under the supervision of the first author. Observers were prepared in four steps. First, the first author gave two introductory sessions on walkability, urban inclusion and sidewalk conditions, with attention to the obstacles produced locally by user behaviour and by poor coordination between public services (roads and utility networks, infrastructure, and urban management). Second, the teams were formed and carried out a preliminary field reconnaissance on Rue Palestine (R5), which was not part of the audit sample. Third, a harmonisation and calibration workshop led by the first author unified the definitions of the audit criteria, so that all

teams interpreted the standardised audit sheet in the same way. Fourth, the survey was carried out on the seven audited axes. For each observation point, the audit sheet recorded the obstacles observed, classified as human-behaviour, infrastructural or natural and as temporary or permanent, together with the side of the street and the time of observation. The protocol combined quantitative counts with systematic photographic documentation of each recorded obstacle; the photographs served to verify and classify the counts, and no separate qualitative analysis was carried out. Its components were as follows.

Visual and photographic survey. Each identified obstacle was photographed at the moment of recording. The photographic record provides empirical support for the count entered in the audit sheet and documents the typology of the obstruction observed. The photographic record is retained by the authors as internal documentation and is not distributed with the dataset.

Observation window. Fieldwork was conducted between 09:00 and 19:00. This period covers the main daytime commercial and pedestrian activity of the district, so that the temporary obstructions generated by human activity—unregulated parking, waste deposits and merchandise placed on the sidewalk—could be observed together with permanent obstacles. The field report of each team gives the time of its visit to each street unit. Except for R6, whose reports give the interval 17:00–19:00, this is a single clock time, which may mark only the start of the visit; the duration of the visits was not recorded. On this basis, the visits to 21 of the 26 street units can be assigned approximately to three periods: eight units (16 sides; R3, R4, and R8_S3) were audited from the morning (recorded times 09:00–11:00), five (10 sides; R1 and R2) from the early afternoon (14:00–14:45) and eight (16 sides; R6, R8_S1, and R8_S2) in the evening peak (17:00–19:00); no visit time was recorded for the five units of R7. Section 4.5 examines the effect of visit time on the results.

Lateral differentiation. Auditing the two sides of each street unit separately (Section 2.1) allows the symmetry or asymmetry of accessibility conditions within a unit to be assessed.

Quality control. All completed audit sheets were reviewed and corrected by the first author against the photographic record, and the first author coded the field categories of the audit sheet into the twenty audit variables defined above, so that the same criteria were applied to every street.

Eight synthetic variables were constructed by grouping the twenty raw variables according to morphological function and the type of municipal response they imply. They are labelled X1–X8 to distinguish them from the two obstruction profiles produced later by *k*-means, C1 (lower obstruction) and C2 (higher obstruction). Each synthetic variable is the sum of the occurrences per 100 m of its constituent variables (Table 1) and is interpreted as a relative burden score within this dataset rather than as a calibrated physical unit.

The grouping follows the municipal service that would act on each problem, so that every family corresponds to a distinct intervention dimension. Structural defects (X1: insufficient width, damaged surfacing, excessive cross-slope and unsuitable curbs) call for sidewalk reconstruction or resurfacing by public-works services. Street furniture (X2: light poles, road signs, column bases and drainage inlets) calls for relocation or redesign of fixed equipment. Normative accessibility (X3: missing tactile paving and access ramps) calls for the compliance works required by Law No. 02-09 [51]. Commercial occupation (X4: market stalls, merchandise, and advertising panels), illegal parking (X5), and construction sites (X8) are problems of use that call for regulation and enforcement, whereas bulky waste (X6: waste, bulky items, debris, and rubbish) calls for collection and waste management. Natural obstacles (X7: street trees) call for maintenance and planting design. Section 4.4 links these dimensions to intervention types.

During data preparation, a raw column initially labelled “inadequate signage” was found to be numerically identical, segment by segment, to tactile_bands + access_ramps.

Retaining it would have duplicated the accessibility dimension, so the duplicate column was removed before analysis; the final audit contains twenty raw variables.

X3 requires a distinct interpretation. It records accessibility-compliance deficits—missing tactile paving and access ramps—which can impede particular users without necessarily occupying sidewalk area. X3 is retained in the obstruction profiles because universal accessibility is a substantive component of pedestrian quality. However, because X3 does not represent physical occupancy in the same way as the other families, the action taxonomy in Section 4.4 is reported both with and without X3.

2.3. Analytical Processing Workflow and Tools

Descriptive statistics and correlation screening were carried out in Orange Data Mining. All other analyses were carried out in R 4.6.1 [52]: principal component analysis; *k*-means partitioning, internal indices, and the gap statistic [53] (packages cluster and fpc); street-unit bootstrap stability [54]; random-forest fitting (ranger) with cross-validation grouped by street unit (rsample); exact TreeSHAP attribution (treeshap) [55]; the decision tree (rpart); and the hierarchical clustering and multidimensional scaling reported in Section 3.2. The agent-based sweep was run in NetLogo (Section 2.5). Robustness checks of the family ordering are reported in Appendix D. The R scripts and the per-100 m data file are provided as Supplementary Materials. The workflow keeps three levels of evidence apart: descriptive patterning in the audit, internal summaries of the fitted partition, and a mechanistic illustration in simulation. It comprises the seven steps listed below and summarised in Figure 2.

1. Step 1—Description. Distribution and variability of the twenty raw audit variables were characterised by descriptive statistics.
2. Step 2—Correlation screening. Pairwise Spearman associations among the raw variables were inspected to detect redundancy.
3. Step 3—Dimensional structure. The eight standardised synthetic variables were submitted to principal component analysis (Figure 3). The PCA is descriptive, and partitioning was not performed on component scores.
4. Step 4—Partitioning. *k*-means (100 random starts) was run on the standardised synthetic variables for k = 2–10; Section 2.4 explains the choice of k and the stability assessment.
5. Step 5—Summary of the partition. A decision tree and a random forest with SHAP attribution were fitted to the *k*-means labels. Because these labels are generated from the same variables, the purpose of this step is not to show that the profiles can be predicted, but to translate the multidimensional partition into terms a municipality can act on: the tree gives a few readable rules, and SHAP shows how much each obstacle family contributes to the separation between profiles and in which range of values it matters. The random forest was evaluated with five-fold cross-validation grouped by street unit (20 repetitions) and with leave-one-street-unit-out validation, so that the two sides of a street unit never fall in different folds [56].
6. Step 6—Priority ordering. Families were ranked by mean absolute SHAP value, averaged over 100 random forests with different random seeds and rescaled to percentages, and the ranking was cross-checked against the univariate between-profile contrasts. Because the ranking describes how strongly each family separates the two profiles, it is treated as an internal interpretive ranking rather than as direct evidence of intervention effectiveness; its robustness to the number of profiles, to grouped resampling, and to time-sensitive families is examined in Appendix D.

7. Step 7—Simulation. A minimal agent-based corridor model was used to illustrate how purely local avoidance can generate nonlinear performance loss as obstruction rises (Section 2.5).

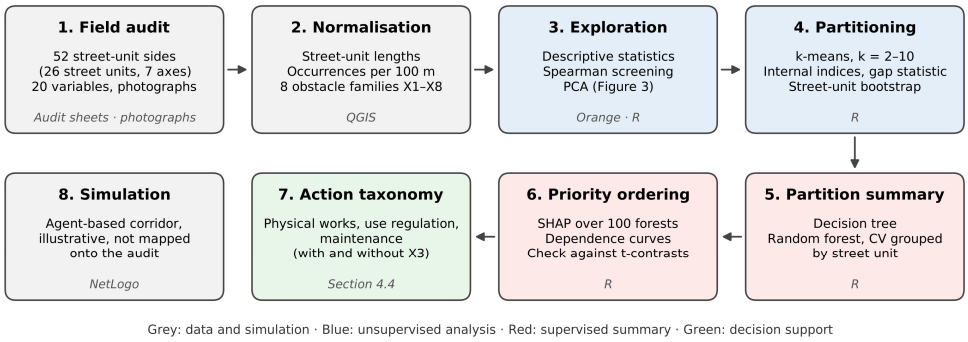


Figure 2. Analytical workflow: field audit and length normalisation, descriptive and dimensional analysis, *k*-means partitioning with stability assessment, summary of the partition by decision tree and random forest with SHAP attribution under grouped validation, action taxonomy, and illustrative agent-based simulation.

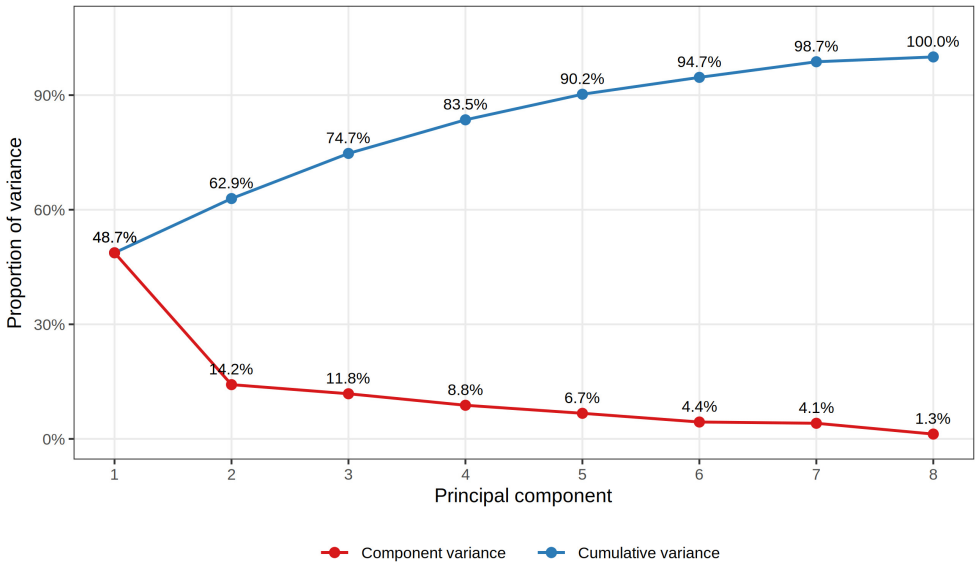


Figure 3. Principal component analysis of the eight standardised synthetic variables (occurrences per 100 m), shown as a scree plot with cumulative variance. Three components carry 74.7% of total variance, with a marked elbow after the first.

In Figure 3, the component-variance curve falls sharply after the first component (48.7%), while the cumulative curve reaches 74.7% by the third. Much of the variation in the eight scores can therefore be represented by a few descriptive dimensions; the PCA is not used to determine *k*.

These observations motivated a multistage design in which obstruction patterns are first stratified and then summarised for interpretation. Pairing unsupervised pattern discovery with supervised summarisation is useful for interpretability when the supervised stage is kept separate from validation [57]. Claims are accordingly restricted to descriptive statements about the sampled district, statements about how the fitted partition is organised, and qualitative statements about mechanism from the agent-based model.

2.4. Choosing k and Internal Assessment of the Partition

The number of clusters was chosen empirically. *k*-means was run on the eight standardised synthetic variables for every *k* between 2 and 10, and each partition was scored on four complementary internal criteria (Table 2). The Calinski–Harabasz index measures the ratio of between-cluster to within-cluster dispersion and favours compact, well-separated partitions; the Davies–Bouldin index measures the average similarity of each cluster to its most similar neighbour, lower values being better; the mean silhouette coefficient measures, for each observation, how much closer it is to its own cluster than to the nearest other cluster, and is directly interpretable at the level of individual street-unit sides; and the gap statistic of Tibshirani et al. [53] compares within-cluster dispersion with that expected under a reference distribution without cluster structure (500 reference datasets). These four indices are widely used and respond to different aspects of cluster structure, so agreement among them is more informative than any single criterion.

Table 2. Internal validity indices for *k*-means partitions of the eight standardised synthetic variables (occurrences per 100 m), $k = 2$ to 10. s_k is the standard error of the gap estimate.

k	Calinski–Harabasz	Davies–Bouldin	Gap	s_k	Silhouette
2	26.23	1.318	0.387	0.027	0.339
3	21.93	1.463	0.418	0.026	0.271
4	19.69	1.367	0.427	0.027	0.281
5	18.41	1.291	0.432	0.027	0.303
6	17.59	1.237	0.445	0.027	0.284
7	16.91	1.114	0.445	0.028	0.284
8	16.17	1.120	0.443	0.028	0.275
9	15.61	1.009	0.453	0.028	0.278
10	15.15	1.067	0.451	0.029	0.235

The silhouette and the Calinski–Harabasz index are highest at $k = 2$ (0.339 and 26.2), whereas the Davies–Bouldin index decreases irregularly with *k* and is lowest at $k = 9$. The gap statistic rises gradually with *k*: applying the decision rule of Tibshirani et al. [53]—retain the smallest *k* for which $\mathrm{Gap}(k) \geq \mathrm{Gap}(k+1) - s_{k+1}$—gives $k = 3$ ($0.418 \geq 0.427 - 0.027$), and the first-SE-maximum rule gives $k = 4$. This pattern indicates weak rather than sharp cluster separation.

We therefore adopt $k = 2$ mainly as an operational prioritisation device: the substantive task is triage, distinguishing lower- from higher-obstruction street-unit sides, for which two ordered profiles are the most useful output. This choice is supported, but not uniquely determined, by the internal indices. Two further checks support it (Section 3.2). First, compared directly with $k = 4$, the two-profile solution scores better on the silhouette, Calinski–Harabasz, and Davies–Bouldin indices. Second, a bootstrap of the 26 street units (1000 replicates, keeping the two sides of each unit together) shows that both $k = 2$ profiles are stable (mean Jaccard similarity 0.89 and 0.83 [54]), whereas two of the four $k = 4$ groups are not reproduced. C1 and C2 are therefore read as ordered strata of obstruction burden rather than as two natural street types.

2.5. Agent-Based Model of the Obstruction Mechanism

To explore a possible behavioural mechanism linking physical blockage to pedestrian performance, we built a deliberately minimal agent-based model in NetLogo [58,59]. The model is not a calibrated representation of Blida. Agents enter one end of a stylised 75×6-cell corridor and move toward the exit using only local avoidance rules: advance if possible, otherwise step diagonally, otherwise move laterally [60–62]. Obstacles occupy a

randomly selected fraction of cells, with density swept from 0 to 0.40 in steps of 0.02. Twenty independent replications per level yielded 420 runs of 2000 ticks. This replication count is sufficient to expose the broad shape of the response but not to locate the transition precisely: near the transition, the level-to-level scatter is of the same order as the differences between adjacent levels. The density sweep is therefore reported as a shape, and no single density value is treated as an estimated threshold. Throughput, effective speed, crossing time, and blocking events were recorded. Because no aggregate density–performance relation is encoded in the rules, any nonlinear response is generated by the local interactions of the model. The mechanism is closely related to site percolation in a narrow strip: as randomly placed obstacles accumulate, the probability that no traversable lateral path remains rises sharply over a narrow density band, and mutual exclusion between agents adds an effective occupancy on top of the obstacle density. The model is therefore best read as an urban-design-facing illustration of a well-characterised lattice phenomenon rather than as the discovery of a new effect; its contribution is to place that phenomenon alongside a field audit, not to establish it.

Two specifications are stated explicitly, because the interpretation in Section 3.5 depends on them.

First, the corridor lattice is dimensionless. A cell is a unit of occupancy rather than a calibrated area, so obstacle density is a fraction of blocked cells and not a measurement in obstacles per square metre. The simulation can therefore support a qualitative mechanism claim and relative comparisons, but it cannot establish a metric threshold for Blida or any other city.

Second, measured throughput depends on the pedestrian inflow regime. The corridor uses a constant injection rate that does not saturate it at density zero, which contributes to the flat throughput region at low obstacle densities. A nonlinear deterioration still emerges under this specification, but both the plateau and the numerical location of the transition may shift under alternative inflow regimes. The transition is therefore interpreted as model-specific rather than universal.

The simulation is not linked numerically to the audit. Audit occurrences differ widely in physical footprint, and the accessibility family X3 records missing provisions rather than occupied space, so no defensible conversion exists between occurrences per 100 m and blocked-cell density. The model is used to illustrate a mechanism: small local detours, each harmless on its own, can add up to a disproportionate loss of pedestrian performance once obstruction passes a model-specific level. This mechanism is the reason the study prioritises street units by their cumulative obstruction profile rather than by any single obstacle type.

Appendix A provides the consolidated specification of the agent-based model.

3. Results

3.1. Descriptive Profile of the Twenty Raw Variables

Table 3 reports descriptive statistics for the 20 raw audit variables, as counts per street-unit side. The largest recorded mean burdens concern missing tactile paving (mean 13.23), damaged surfacing (5.48), insufficient width (4.46), and light poles (4.54). Informal appropriation is represented by unauthorised parking (mean 2.69) and market stalls (mean 2.50). Dispersion is high for several variables, with maxima far above medians, indicating a right-skewed distribution of recorded obstruction burden.

Table 3. Descriptive statistics for the twenty raw variables (N = 52 street-unit sides from 26 street units). Counts are recorded as audit occurrences per street-unit side before length normalisation; all subsequent analyses use occurrences per 100 m (Section 2.1).

Variable	Description	Mean	Median	Min–Max
insuff_wid	insufficient usable width	4.46	2	0–20
damag_coat	damaged pavement surface	5.48	4	0–21
exces_bank	excessive cross-slope	0.44	0	0–6
unsuitable_borders	unsuitable curb/edge condition	1.23	1	0–8
light_poles	light poles intersecting clear path	4.54	3	0–17
road_signs	road signs intersecting clear path	1.12	1	0–4
trees	trees intersecting clear path	2.63	1	0–15
mouth_sewer	sewer/drainage inlets	2.10	2	0–10
column_bases	column bases	1.77	1	0–7
tactile_bands	missing tactile paving	13.23	11.5	2–40
access_ramps	missing access ramps	5.12	4	0–12
march_shops	market stalls	2.50	1.5	0–14
merchandise	merchandise encroachment	1.54	1	0–5
advertising_panels	advertising panels	0.65	0	0–4
anarchic_park	unauthorised parking	2.69	1	0–15
waste_garbage	waste/garbage accumulation	2.19	2	0–6
bulky_items	bulky items	2.06	2	0–10
rubbish	loose rubbish	0.42	0	0–3
debris	debris	0.42	0	0–3
work	construction worksites	0.46	0	0–3

Table 4 summarises the eight synthetic variables in occurrences per 100 m. The heaviest average burden falls on normative accessibility (X3, 4.60 deficits per 100 m), ahead of structural defects (X1, 3.10) and street furniture (X2, 2.47).

Table 4. Descriptive statistics for the eight synthetic variables X1–X8 across the 52 street-unit sides, in occurrences per 100 m (X3: deficits per 100 m). These scores are the inputs to the partitioning and attribution analyses. The action-class column identifies the type of intervention associated with each family (Section 4.4).

Synthetic Variable	Action Class	Mean (/100 m)	Median	Min–Max
X1 Structural defects	Physical works	3.10	2.45	0–9.71
X2 Street furniture	Physical works	2.47	2.27	0.24–6.46
X3 Normative accessibility	Physical works	4.60	4.29	0.46–12.62
X4 Commercial occupation	Use regulation	1.23	0.69	0–6.25
X5 Illegal parking	Use regulation	0.65	0.38	0–3.62
X6 Bulky waste	Use regulation	1.36	1.18	0–4.72
X7 Natural obstacles	Maintenance	0.53	0.34	0–2.85
X8 Construction sites	Use regulation	0.13	0	0–1.04

3.2. Operational k-Means Stratification (k = 2)

With k fixed operationally at two (Section 2.4), k-means on the standardised per-100 m densities returned two ordered obstruction profiles. C1, the lower-obstruction profile, contains 31 street-unit sides (59.6%); C2, the higher-obstruction profile, contains 21 (40.4%). A Ward hierarchical clustering of the same standardised densities (Figure 4) partly recovers the partition (adjusted Rand index = 0.42): one branch holds 22 sides, all in C1, and the other holds all 21 C2 sides together with 9 C1 sides. Figure 5 projects the same distance matrix in two dimensions; the two profiles separate along the first dimension, with transitional sides near the boundary. The silhouette analysis indicates weak and uneven cohesion: 0.339 overall, 0.526 for C1, and 0.063 for C2 (Figure 6). Seven of the 21 C2 sides have negative silhouettes, so C2 combines a core of highly obstructed sides with transitional sides close to C1.

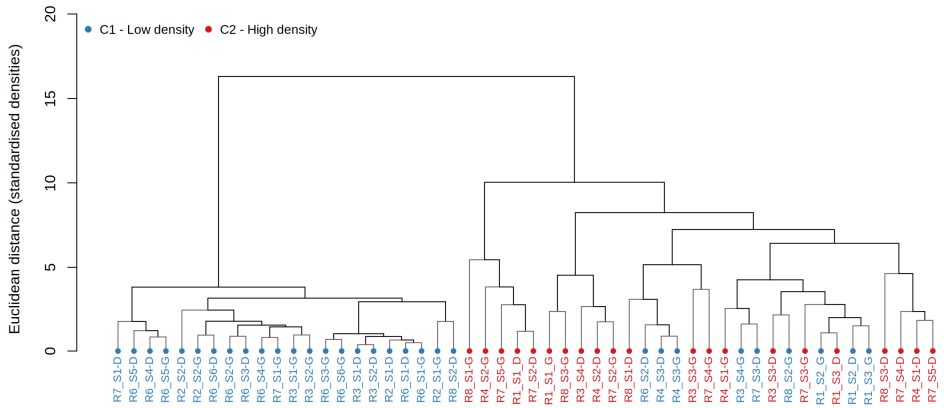


Figure 4. Ward dendrogram of the 52 street-unit sides (Euclidean distance on the eight standardised per-100 m densities). Leaf labels are coloured by *k*-means profile (blue: C1, lower obstruction; red: C2, higher obstruction).

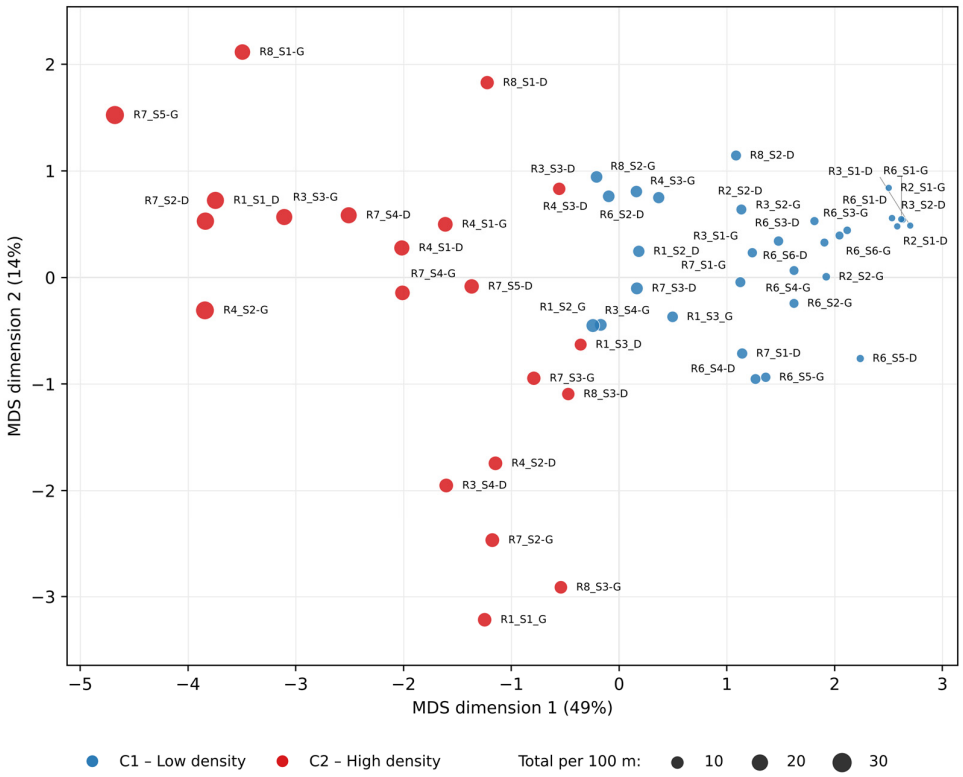


Figure 5. Classical multidimensional scaling of the distance matrix used in Figure 4. Colour gives the *k*-means profile and point size the total occurrences per 100 m. Axes are dimensionless (dimension 1: 49% of the variance; dimension 2: 14%).

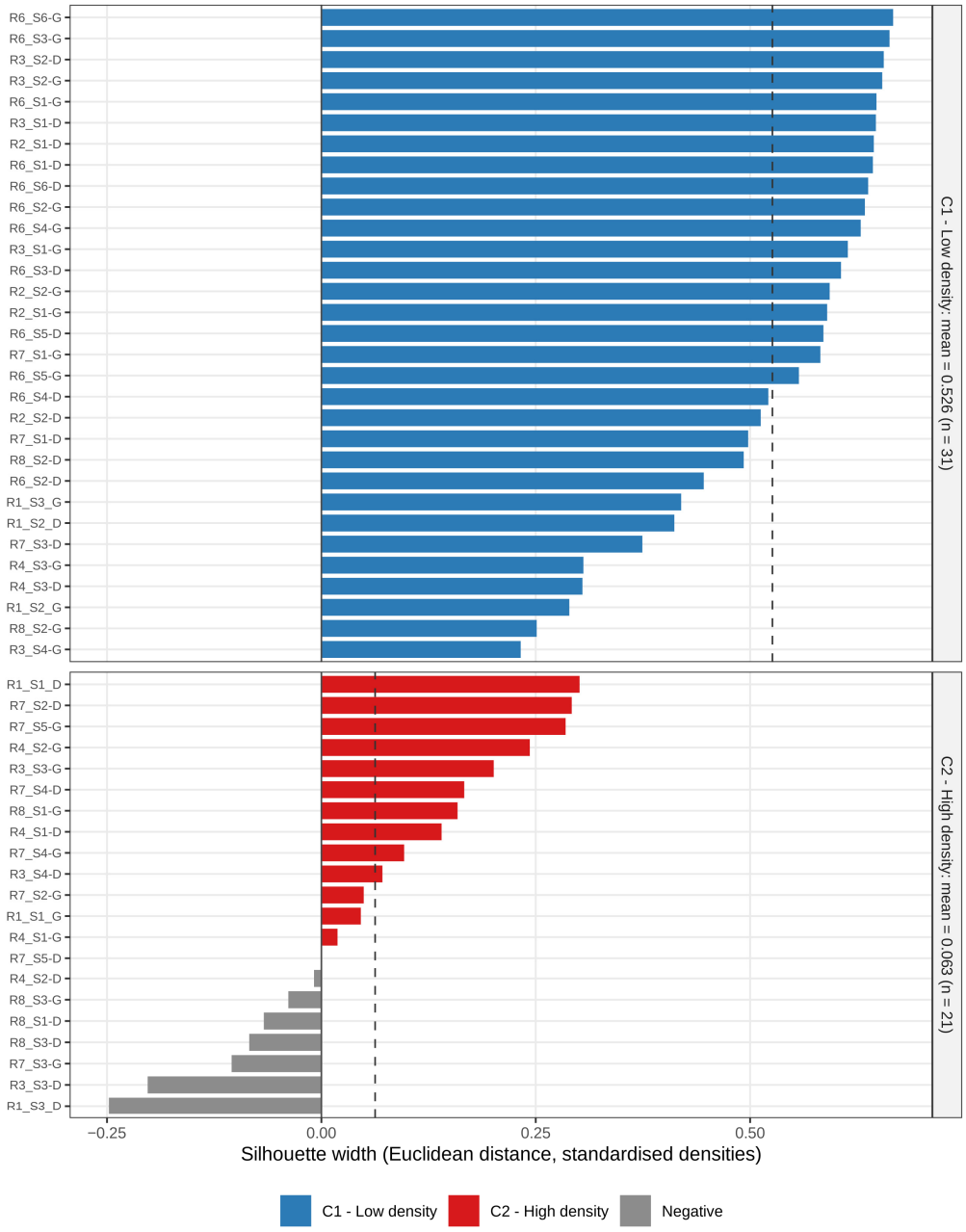


Figure 6. Silhouette widths of the 52 street-unit sides for the two-profile partition. Bars are grouped by profile and sorted; dashed lines mark the profile means (C1 = 0.526; C2 = 0.063; overall = 0.339). Grey bars are the seven C2 sides with negative silhouettes, which lie closer to C1 than to their own profile.

Nominal Student's *t*-statistics describe the magnitude and ordering of separation between the two profiles (Figure 7). All eight synthetic variables differ: normative accessibility (X3: 2.86 vs. 7.16 per 100 m, $t = 8.44$), bulky waste (X6: 0.80 vs. 2.18, $t = 7.51$), structural defects (X1: 1.80 vs. 5.01, $t = 6.12$), street furniture (X2: 1.67 vs. 3.65, $t = 5.54$), illegal parking (X5: 0.27 vs. 1.21, $t = 4.74$), commercial occupation (X4: 0.58 vs. 2.19, $t = 4.11$), natural obstacles (X7: 0.32 vs. 0.85, $t = 3.05$), and construction sites (X8: 0.07 vs. 0.22, $t = 2.43$). All contrasts remain below 0.05 after Holm–Bonferroni adjustment. Because the profiles were generated from the same variables and paired sides are not independent, these statistics describe the partition rather than test hypotheses.

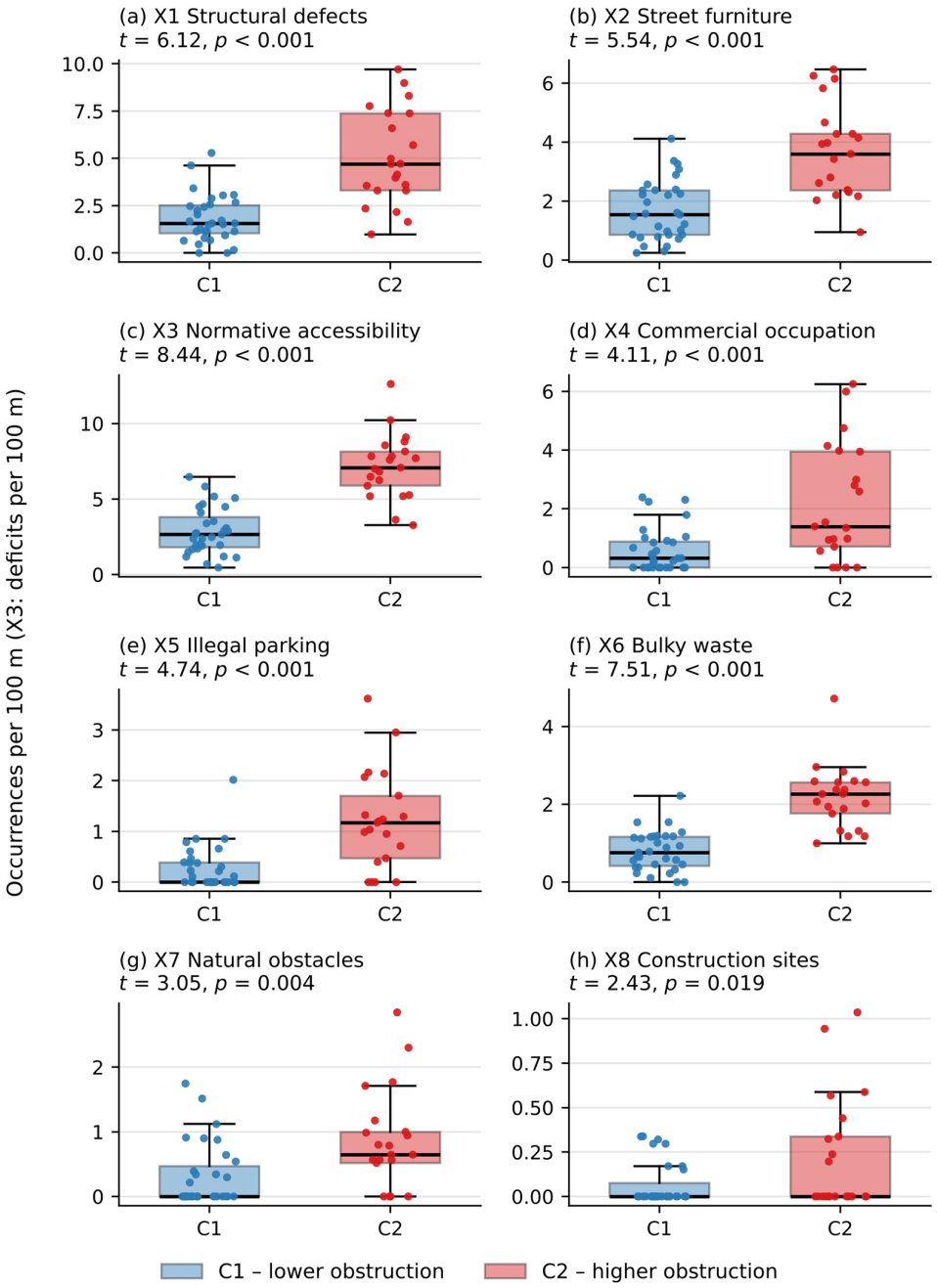


Figure 7. Distribution of the eight synthetic variables (occurrences per 100 m) across the two profiles (N = 52 street-unit sides): (**a**) structural defects; (**b**) street furniture; (**c**) normative accessibility; (**d**) commercial occupation; (**e**) illegal parking; (**f**) bulky waste; (**g**) natural obstacles; (**h**) construction sites. The nominal Student t-statistic and its uncorrected p-value are printed above each panel; Holm-adjusted values are reported in Section 3.2.

Normalisation by length changes the partition materially. The per-100 m solution agrees only weakly with the solution obtained on raw counts (adjusted Rand index = 0.10), and 17 of the 52 sides change profile: the seven sides that move from C2 to C1 belong to long street units (mean 697 m), and the ten that move from C1 to C2 belong to short ones (mean 218 m) (Appendix C). This is the exposure effect that normalisation removes; all results reported here use the normalised densities.

Table 5 compares the two-profile and four-profile solutions, including their stability under the street-unit bootstrap described in Section 2.4. The k = 4 solution separates a low-density group (22 sides), a dense core (7 sides) and a small group marked by construction

sites and street furniture (5 sides), but its fourth group (18 sides) mixes sides from both $k = 2$ profiles, has a near-zero silhouette (0.01) and is not reproduced under resampling.

Table 5. Comparison of the two-profile and four-profile *k*-means solutions on the standardised per-100 m densities. Jaccard similarities are means over 1000 bootstrap replicates of the 26 street units; following Hennig [54], values above 0.75 indicate stable clusters and values of 0.5 or below indicate dissolved clusters.

Criterion	$k = 2$	$k = 4$
Mean silhouette	0.339	0.281
Calinski–Harabasz	26.2	19.7
Davies–Bouldin (lower is better)	1.32	1.37
Profile sizes	31/21	22/18/5/7
Mean Jaccard per profile	0.89; 0.83	0.86; 0.50; 0.61; 0.71
Mean adjusted Rand index (bootstrap)	0.74	0.63

3.3. Decision Tree: Interpretable Sample-Specific Rules

The decision tree (Figure 8) was fitted as a readable summary of the partition, with at least two observations per leaf and no split of nodes with fewer than five observations.

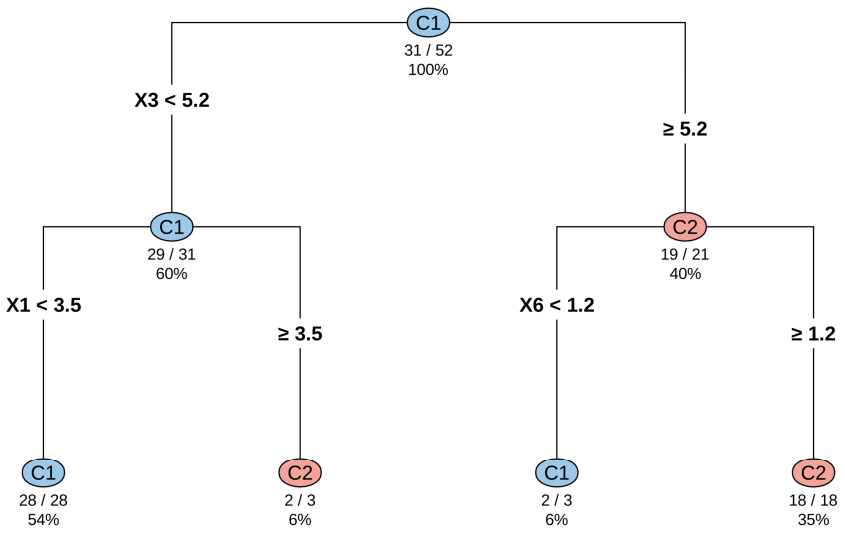


Figure 8. Decision-tree summary of the two-profile partition on per-100 m densities, with splits at X3 $\geq$ 5.2 deficits/100 m, X1 $\geq$ 3.5 and X6 $\geq$ 1.2 obstacles/100 m. Below each node: sides of the predicted profile over all sides in the node, and the node's share of the sample.

The first split occurs at 5.2 normative-accessibility deficits per 100 m. Below it, sides with fewer than 3.5 structural defects per 100 m form a pure C1 leaf (28 of 28); above it, sides with at least 1.2 bulky-waste items per 100 m form a pure C2 leaf (18 of 18). Two small mixed leaves hold the remaining six sides. The tree reproduces 96.2% of the *k*-means labels on the fitted sample but 78.6% (range 73.1–86.5%) under cross-validation grouped by street unit, so its cut-points summarise this sample rather than provide transferable thresholds. Its value is to show how the audit could be compressed into a short screening sequence—accessibility first, then structural defects or bulky waste—once calibrated locally.

3.4. Internal Contribution Ordering of the Eight Obstacle Families

Table 6 reports the internal ordering of the eight obstacle families, measured by mean absolute SHAP values, together with the univariate between-profile contrasts of Section 3.2. The random forest reconstructs the partition well under cross-validation grouped by street unit (Table 7); grouping lowers accuracy and the Matthews correlation coefficient only

modestly relative to folds that ignore street units, which indicates limited leakage between paired sides.

Table 6. Internal attribution ordering of the eight obstacle families: mean absolute Shapley values (exact TreeSHAP [55]) of the random forest, averaged over 100 fits with different random seeds (100 trees, maximum depth 15, minimum node size 5), aggregated across classes and normalised to 100%. Brackets give the 2.5–97.5% range across fits. The right-hand column gives the action class used in Section 4.4.

Synthetic Variable	SHAP Importance, Mean % [2.5–97.5%]	Action Class
X3 Normative accessibility	27.3 [23.0–32.4]	Physical works
X6 Bulky waste	22.6 [19.1–26.4]	Use regulation
X1 Structural defects	15.9 [12.0–19.7]	Physical works
X5 Illegal parking	14.8 [11.4–18.4]	Use regulation
X2 Street furniture	6.2 [3.8–8.2]	Physical works
X4 Commercial occupation	5.4 [3.8–7.2]	Use regulation
X7 Natural obstacles	5.1 [3.4–7.2]	Maintenance
X8 Construction sites	2.6 [1.5–3.7]	Use regulation
Total physical works (X1 + X2 + X3)	49.4	—
Total use regulation (X4 + X5 + X6 + X8)	45.4	—
Total maintenance (X7)	5.1	—

Table 7. Reconstruction of the two-profile partition by the random forest under three validation schemes (means over 20 repetitions for the grouped and stratified schemes). Grouped folds keep the two sides of a street unit together.

Metric	Grouped 5-Fold, Street Units (Main)	Leave-One-Street-Unit-Out	Stratified 5-Fold, Sides
AUC	0.968	0.972	0.976
Overall accuracy	0.900	0.865	0.921
F1 (weighted)	0.900	0.865	0.921
Matthews correlation coefficient	0.794	0.719	0.840

Three families carry the leading attribution weights: normative accessibility (27.3%), bulky waste (22.6%), and structural defects (15.9%), together about two-thirds of the model attribution. X3 ranks first in 90% of the 100 fits. The intervals of structural defects and illegal parking (14.8%) overlap, so these two form a shared third tier. Street furniture (6.2%), commercial occupation (5.4%), natural obstacles (5.1%), and construction sites (2.6%) carry smaller weights. SHAP dependence plots (Figure 9) show threshold-like effects: attribution towards C2 rises sharply between about 4 and 6 accessibility deficits per 100 m, 1 and 1.6 bulky-waste items per 100 m, and 2.5 and 3.5 structural defects per 100 m, and is nearly flat outside these ranges.

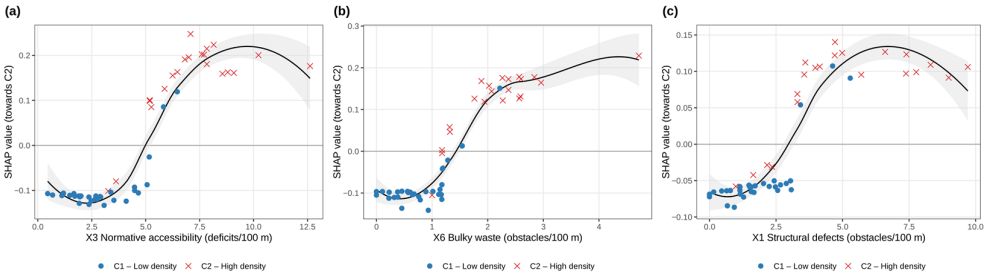


Figure 9. SHAP dependence plots for the three leading families: (**a**) normative accessibility, (**b**) bulky waste, (**c**) structural defects. Each point is a street-unit side; the vertical axis is its mean SHAP value over 100 random-forest fits (positive values push towards C2, the higher-obstruction profile). Curves are LOESS smooths with 95% confidence bands.

The concordance between the two orderings is close but not exact. Ranking the eight families by their between-profile *t*-statistics reproduces the SHAP order except for one adjacent swap between street furniture and illegal parking (Spearman $\rho = 0.98$; Pearson $r = 0.92$). The supervised stage therefore adds interpretive structure, notably the threshold shape of the effects, but little independent discriminatory evidence beyond the simpler contrasts.

The ordering was checked in three further ways (Appendix D, Table A3). First, under the four-profile solution normative accessibility still ranks first (21.5%), but street furniture (18.7%) and illegal parking (16.0%) move ahead of bulky waste (11.2%) and structural defects (10.4%), because the four-profile solution isolates a small group defined by street furniture and construction sites; the rank correlation between the two orderings is 0.69. Second, refitting the random forest within each training set of the grouped cross-validation (100 fits) keeps normative accessibility in the top three families in every fit and first in 77% of fits, and bulky waste in the top three in 99%, while structural defects (65%) and illegal parking (34%) share the third place; the first split of the decision tree falls on normative accessibility in 76% of the training sets and on bulky waste in 17%. Third, a partition built only on the time-insensitive families (X1, X2, X3, X7, and X8) assigns 88% of the street-unit sides to the same profile as the main partition. Normative accessibility is therefore a robust leading dimension, whereas the relative position of the second-tier families depends on the operational partition and should be read with caution.

3.5. Agent-Based Exploration of a Possible Obstruction Mechanism

Across 420 simulations, three model-specific regimes are visible (Table 8, Figure 10). Below approximately 0.26 blocked-cell density, throughput remains close to the free-flow reference but is not monotonic. With only 20 replications per level, individual levels fluctuate by several percentage points in both directions (Figure 10); these fluctuations are replication noise rather than structure. Effective speed declines more smoothly. Deterioration becomes systematic between the 0.26 and 0.30 levels: at 0.30, throughput has fallen to 90.3% and effective speed to 77.9% of free flow, followed by a steep drop at 0.32 (68.7% throughput; 57.7% effective speed). Performance continues to decline at higher densities. For clarity, we distinguish a noisy low-density region ($\leq$0.26), a transition between 0.26 and 0.30, and a steep collapse region beyond 0.32. These boundaries are indicative and describe this model specification only.

Table 8. Emergent throughput and effective speed as functions of blocked-cell density in the agent-based model (20 replications per level; values normalised to free flow). Selected levels are tabulated; the complete 21-level sweep is plotted in Figure 10. † Values above 100% in the low-density region reflect replication noise at 20 replications per level.

Obstacle Density	Throughput (% Free-Flow)	Effective Speed (% Free-Flow)
0.00	100.0	100.0
0.14	100.2 †	98.6
0.20	100.8 †	96.6
0.26	100.4 †	94.3
0.30	90.3	77.9
0.32	68.7	57.7
0.36	58.9	46.3
0.40	24.2	19.0

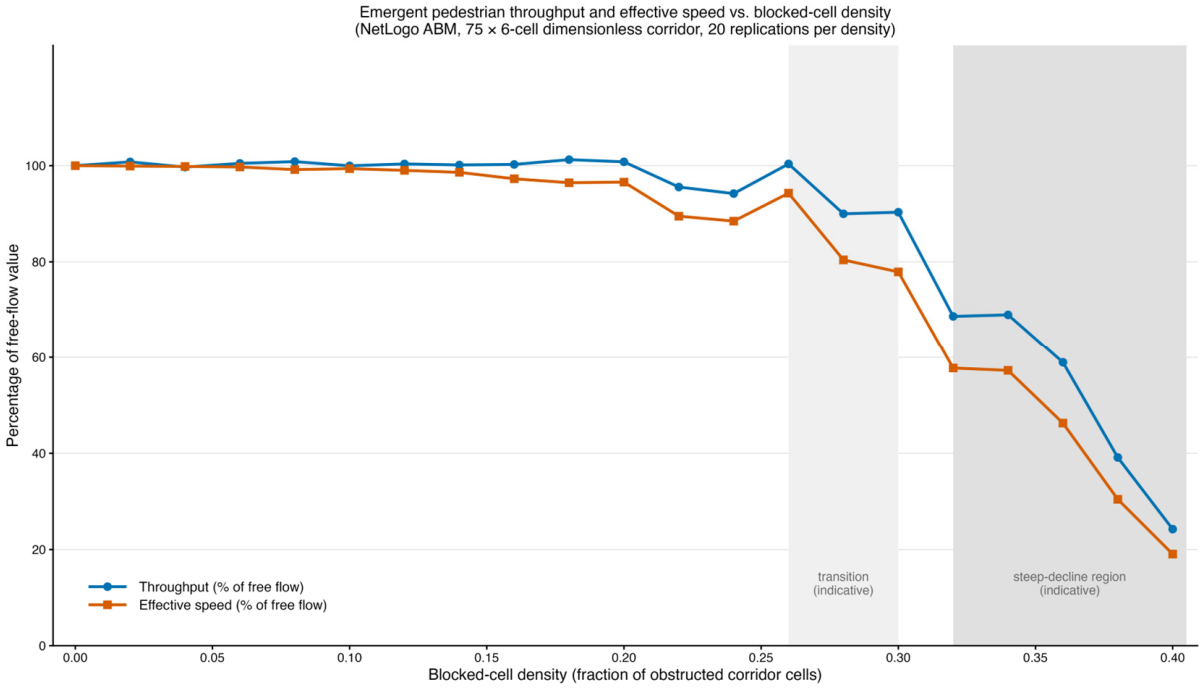


Figure 10. Emergent pedestrian throughput and effective speed versus blocked-cell density in the agent-based model (75 × 6-cell corridor; 20 replications per density). Shaded bands mark the indicative transition and steep-decline regions described in Section 3.5.

Table 8 reports selected levels of the density sweep.

Because the model encodes only local avoidance and no aggregate density–throughput curve, the nonlinear deterioration is an emergent property of this simplified specification. The result supports the qualitative proposition that accumulated local detours can generate disproportionate performance loss; it does not establish the numerical location of such a transition in Blida.

Because the corridor is dimensionless, the empirical profiles C1 and C2 are not placed on the simulated curve. The simulation is used to illustrate mechanism and nonlinearity, not to state whether any sampled street has crossed a real-world capacity threshold.

Mean crossing time is not used as an indicator here, since at high density it is biased downward: only agents on the least-obstructed paths ever complete the corridor.

In summary, Section 3 shows that the per-100 m audit supports an operational two-profile reading, that three families (accessibility deficits, bulky waste, and structural defects) drive the separation through threshold-like effects, and that obstruction can degrade pedestrian performance nonlinearly in the simulated corridor.

4. Discussion

4.1. Interpretation of Urban Segmentation

The *k*-means analysis provides a pragmatic two-profile summary of the 52 street-unit sides: C1 (59.6%) represents lower recorded obstruction, and C2 (40.4%) represents higher recorded obstruction. The profiles are stable under street-unit resampling, but C2 is internally heterogeneous, so C1 and C2 are best read as operational strata of obstruction burden rather than as natural street types.

The higher-obstruction profile shows a broad escalation across all audit families rather than dependence on a single obstacle type. Accessibility deficits (t = 8.44), bulky waste (t = 7.51) and structural defects (t = 6.12) show the largest contrasts, whereas illegal parking (t = 4.74), which led the separation when counts were not normalised, becomes secondary

once exposure is accounted for. Informal appropriation is therefore one of several concurrent dimensions of obstruction, alongside structural deficiencies, accessibility deficits and the management of waste [63,64].

4.2. Role of the Supervised Stage

The two profiles are readily encoded by the variables that generated them: three decision-tree splits reproduce most of the fitted sample (Section 3.3), and the random forest reconstructs the labels with an accuracy of 0.90 under cross-validation grouped by street unit (Table 7). These results show that the partition is internally coherent and robust to the dependence between paired sides; because the labels derive from the same variables, they do not constitute external validation.

The near-identical agreement between the SHAP ranking and the univariate contrast ranking reinforces the same reading. The supervised stage does not reveal a hierarchy hidden from simpler statistics; its contribution is to show where each family starts to matter, through the threshold-like dependence curves, and to provide a compact rule set. Applied urban-analytics studies that predict unsupervised labels from the same features should keep this distinction between reconstruction and validation explicit [47].

What the analysis contributes is a transparent route from a street-level audit to an ordered set of intervention families. The decision tree shows how a few audit dimensions can compress the partition into readable rules, and the attribution ordering shows how obstruction burden is distributed across those dimensions; operational use of either would require local calibration.

4.3. Exploratory Simulation and Implications for Intervention

The decision tree yields sample-specific cut-points that describe how the partition is organised: about 5.2 accessibility deficits per 100 m at the first split, followed by 3.5 structural defects or 1.2 bulky-waste items per 100 m. The SHAP dependence curves place the steepest changes in similar ranges. These values identify which dimensions deserve attention first; they are not calibrated intervention thresholds.

The agent-based model provides a separate mechanistic exploration. Under the stated corridor and inflow assumptions, purely local avoidance produces a nonlinear deterioration in throughput and effective speed once blocked-cell density becomes sufficiently high. This qualitative result is consistent with evidence that built-environment effects can be nonlinear and interactive [65–67], while remaining explicitly model-specific.

The simulation is deliberately not mapped onto the audit (Section 2.5). Its policy implication is qualitative: because performance can collapse once local detours accumulate, preventing the accumulation of several obstruction types on the same sidewalk is preferable to waiting for severe blockage.

Using the model operationally would require behavioural field data—pedestrian counts, observed detours or carriageway incursions—and corridors matched to measured sidewalk widths and obstacle footprints [62,68,69].

The accessibility dimension remains important independently of the simulation because it reflects statutory and rights-based obligations. X3 aligns with Algerian Law No. 02-09 of 8 May 2002 on the protection and promotion of persons with disabilities [51] and with the United Nations Convention on the Rights of Persons with Disabilities [70]. Informal commerce (X4), by contrast, raises a governance question as well as a spatial one [71,72]. The decision-support value of the analysis is therefore in combining these distinct intervention logics, not in reducing them to a single physical threshold.

4.4. Prioritisation by Intervention Type: A Three-Class Action Taxonomy

Section 3.4 places normative accessibility, bulky waste and structural defects at the top of the internal ordering, followed by illegal parking, with the remaining four families well behind. Because the ordering closely matches the univariate contrast ordering, it is read as a summary of priority dimensions in the sampled profiles. It is an internal interpretive ranking: it shows which families distinguish the higher-obstruction sides in this sample, not that intervening on these families yields the largest gains for pedestrians, which would require independent evidence such as expert assessment or observed pedestrian behaviour.

One methodological point must be settled before the weights are interpreted. Whether "governance" or "infrastructure" appears dominant depends entirely on how the eight families are grouped. The highest-ranked family, accessibility (X3), is addressed by physical works—installing tactile paving and ramps—whereas parking (X5) is addressed by regulation and enforcement. Any binary "governance versus infrastructure" verdict is therefore an artefact of labelling rather than an empirical finding, and we deliberately avoid it.

We instead group obstacle families by the type of intervention each requires, using a three-class action taxonomy (Table 6). Physical works—structural repair, furniture relocation and accessibility compliance (X1 + X2 + X3)—carry 49.4% of attribution. Regulation of use—parking, commerce, waste, and worksites (X4 + X5 + X6 + X8)—carries 45.4%. Routine maintenance of natural obstacles (X7) carries 5.1%. The ranking remains sensitive to grouping choices, which are therefore stated explicitly.

Because X3 counts required-but-missing provisions rather than objects occupying the sidewalk (Section 2.2), we report the same taxonomy with X3 removed and the remaining attribution renormalised to 100%. Use regulation then accounts for 62.5%, physical works for 30.4% and maintenance for 7.1%; within use regulation, bulky waste (31.1%) outweighs illegal parking (20.4%). With X3 included, physical works and use regulation are nearly balanced; with X3 excluded, use regulation clearly leads. The two readings answer different questions: the all-variable taxonomy addresses the total compliance and obstruction burden borne by pedestrians, whereas the X3-excluded taxonomy addresses where the sidewalk is physically occupied today. Both are reported as co-primary results, because the choice between them is a policy choice about what counts as an obstruction, and it changes which municipal service leads the response.

Read as decision support, the results suggest that obstruction in central Blida is produced jointly by accessibility deficits, waste and structural deficiencies, and the regulation of informal uses. Table 9 links each obstacle family to the corresponding intervention type, the lead service, and its internal priority in this audit. Three practical implications follow. First, accessibility compliance should be phased towards street-unit sides with the highest X3 burden, because it is a legal obligation rather than a discretionary amenity. Second, bulky-waste management and the enforcement of parking rules are lower-cost actions that can be applied quickly through routine services and negotiated allocation of sidewalk space [73]. Third, structural reconstruction should be targeted at locations where width, surface, or curb conditions materially constrain passage, while conflicts with fixed equipment can often be solved by relocation rather than reconstruction. These priorities apply to the audited district; site-level implementation should follow local inspection.

Table 9. Obstacle families, corresponding intervention types, and internal priority in the audited district. Internal priority follows the mean SHAP attribution (Table 6): high, ≥20%; medium, 10–20%; low, <10%. It ranks families by how strongly they separate the two obstruction profiles and should be confirmed with independent evidence before it is used to allocate budgets.

Obstacle Family	Main Problems Recorded	Intervention Type	Lead Service	Internal Priority (SHAP)
X3 Normative accessibility	Missing tactile paving and access ramps	Accessibility compliance works (Law No. 02-09)	Public works; accessibility programme	High (27.3%)
X6 Bulky waste	Waste deposits, bulky items, debris, rubbish	Collection, waste management, enforcement against dumping	Municipal cleansing services	High (22.6%)
X1 Structural defects	Insufficient width, damaged surface, cross-slope, unsuitable curbs	Sidewalk reconstruction and resurfacing	Public works	Medium (15.9%)
X5 Illegal parking	Vehicles parked on the sidewalk	Parking enforcement; physical protection (bollards)	Municipal police; traffic services	Medium (14.8%)
X2 Street furniture	Light poles, signs, column bases, drainage inlets	Relocation or redesign of fixed equipment	Public works; utility operators	Low (6.2%)
X4 Commercial occupation	Stalls, merchandise, advertising panels	Designated vending areas; negotiated rules; permits	Trade and public-space services	Low (5.4%)
X7 Natural obstacles	Street trees within the walking zone	Maintenance; tree-pit and planting design	Parks and green-space services	Low (5.1%)
X8 Construction sites	Works occupying the sidewalk	Permits with mandatory pedestrian diversion	Planning and permit services	Low (2.6%)

4.5. Methodological Limitations, Validity Boundaries and Generalisability

The following limitations define the scope of the study.

Sampling and dependence. The dataset contains 52 street-unit sides nested within 26 street units in one central commercial district. Paired sides share contextual characteristics and are not fully independent, so the effective information is closer to 26 units than to 52 observations. Bootstrap stability and random-forest validation were therefore carried out at the street-unit level (Sections 2.4 and 3.4), but the descriptive t-statistics remain nominal. The small sample also exposes the supervised stage to overfitting: with about 26 independent units, a flexible classifier can fit the idiosyncrasies of individual sides. This risk was limited by a minimum node size of five, by averaging over 100 fits, and by evaluating the random forest only on held-out street units (accuracy 0.900 under grouped folds and 0.865 under leave-one-street-unit-out validation; Table 7). The decision tree is more affected, reproducing 96.2% of the fitted labels but 78.6% under grouped cross-validation, so its cut-points are sample-specific. The family ordering is less exposed, because it matches the univariate contrasts ($\rho = 0.98$) and remains stable across grouped training sets (median $\rho = 0.95$; Appendix D); it nevertheless summarises this sample and is not intended to predict conditions in other districts.

Measurement scale. Counts were normalised per 100 m of sidewalk using digitised street-unit lengths, which removes the main exposure effect (Appendix C). Length does not capture sidewalk width, so obstacles per square metre or an effective-clear-width measure would provide a stronger basis for comparing streets of different geometry.

Spatial structure. The sampled units are spatially concentrated and partly contiguous within one commercial district, so spatial dependence may be present. No spatial autocorrelation test or spatially blocked validation was undertaken. The study therefore makes no claim that the fitted internal reconstruction metrics generalise to unsampled neighbourhoods; future multi-area studies should examine spatial dependence explicitly.

Cluster support. The internal indices favour $k = 2$, whereas the gap statistic favours $k = 3$ or 4, and the mean silhouette of C2 is only 0.063. The two-profile solution is stable under street-unit bootstrap resampling, but it is used as an operational prioritisation device rather than as evidence that the streets form two natural populations; replication in other districts is needed before the structure is generalised.

Circularity of the supervised stage. The random-forest labels are derived from the same variables used as predictors, so the classifier, decision tree, and SHAP values summarise the clustering rather than validate it against an external criterion, and the SHAP ordering is an internal interpretive ranking rather than a measure of intervention effectiveness. External validation would require an independent outcome, such as expert ratings, observed pedestrian behaviour, or a separately collected sample.

Construct validity of the accessibility family. X3 is the family with the largest between-profile contrast ($t = 8.44$) and the largest mean SHAP attribution (27.3%), so it materially influences the priority ordering. Unlike the other families, X3 enumerates required-but-missing provisions rather than present objects, and it may still scale nonlinearly with length after normalisation. It is therefore interpreted as a compliance burden, and the X3-excluded taxonomy in Section 4.4 is reported as a co-primary reading.

Inter-rater reliability. All audit sheets were reviewed against the photographic record and coded into the 20 variables by a single person, the first author, which ensures that the same criteria were applied across streets and teams; all observers had followed the same preparation and calibration workshop and used the same standardised audit sheet. No inter-rater coefficient is available; however, neither an independent re-audit nor a blind re-coding of the photographs by a second coder could be carried out within this study, and a single-coder review, while improving consistency, is not an independent reliability check.

Time of day. The families that record temporary occupation—commercial occupation (X4), illegal parking (X5), and bulky waste (X6)—are sensitive to the hour of observation, and the recorded counts are not adjusted for it. The visit times recorded for 21 street units (Section 2.2) allow a partial check. Units audited in the evening peak did not show higher densities of these families than units audited in the morning or early afternoon (street-unit medians in the morning, early afternoon and evening peak, in occurrences per 100 m: X4, 0.48, 1.18, and 0.40; X5, 0.44, 0.85, and 0.25; X6, 1.32, 1.41, and 0.76; Kruskal–Wallis $p = 0.31$, 0.64, and 0.24), and 14 of the 16 sides audited at the peak belong to the lower-obstruction profile (Fisher's exact test, $p = 0.03$ by side and 0.22 by street unit). These comparisons are approximate: the recorded times may mark only the start of a visit, and long visits may extend into the following period, which would tend to blur differences between periods. Visit time is also confounded with street, because every street except R8 has a single recorded time, so these comparisons cannot separate an effect of the hour from differences between streets; the visit time of R7 was not recorded. A partition built only on the time-insensitive families assigns 88% of the street-unit sides to the same profile and keeps normative accessibility and structural defects at the top of the ordering (Appendix D). These checks give no indication that visit time drives the main result, but they cannot exclude it; repeat visits to the same street units at fixed hours, or paired peak and off-peak audits, would separate temporary from permanent obstruction. Because bulky waste (X6), the second family in the ordering, is time-sensitive, its position should be read with particular caution.

Simulation. The agent-based corridor is dimensionless and intentionally simplified; it is not mapped onto field densities, obstacle footprints are treated uniformly, positions are random, and the throughput plateau depends on the inflow specification. The simulation therefore supports a mechanism-oriented claim only; behavioural and geometric calibration would be required before any simulated value could guide municipal action.

Design. The field audit is cross-sectional, so it cannot establish temporal stability, causal effects, or the performance of interventions. Longitudinal and before-and-after designs on treated and untreated locations are needed to evaluate intervention effectiveness.

4.6. Implications for Future Research and Public Policy

This decision-support approach is transferable primarily as a workflow rather than as a set of numerical thresholds. For Blida, the current evidence supports pilot actions that combine accessibility compliance, relocation or redesign of obstructive street equipment, and management of parking, commerce, and waste in the higher-burden street-unit sides. In other North African or resource-constrained cities, the same audit-to-prioritisation sequence could be applied after adapting variable definitions and recalibrating any decision rules to local geometry and governance conditions [39,40,74]. Two cautions attach to that transfer. Street morphology varies systematically across African cities, so audit units and aggregation rules calibrated in Blida should not be assumed comparable elsewhere without checking the underlying form [75]. And analytic instruments of this kind carry a governance risk as well as a governance promise: transferred without local adaptation, data-driven urban tools can substitute technical ranking for political deliberation about who public space is for [76].

Three policy directions follow without relying on the simulated density as a field standard. First, a municipal public-space unit could monitor and reduce high obstruction-burden scores, with particular attention to accessibility deficits and fixed elements that narrow the clear sidewalk width. Second, informal commerce should be managed through designated locations and negotiated rules rather than treated only as a removal problem, while unauthorised parking requires routine enforcement. Third, a simple periodic audit of the leading dimensions (X3, X6, and X1) could be used to rank locations for inspection and intervention. The three-rule decision tree demonstrates the potential simplicity of such a screening tool, but its numerical cut-points require independent local calibration before operational adoption.

From a sustainability perspective, most of the priorities identified here are low-cost and quick to implement. Once accessibility deficits are set aside, use-regulation actions—waste collection, parking enforcement and the management of commercial uses and worksites—account for 62.5% of the attribution and can be delivered by existing municipal services without major capital investment, while accessibility compliance and structural repair can be phased within public-works programmes. Such a sequence restores walkable space quickly, supports a shift towards low-carbon mobility in the city centre and advances inclusive access for vulnerable users, which makes the protocol a practical tool for the local implementation of Sustainable Development Goal 11 [50].

Before operational deployment, the framework would need an independent reliability check, area-based normalisation, an external outcome against which the profiles can be validated, a calibrated pedestrian model, and before-and-after evaluation of interventions; these directions are set out in Section 5. For the agent-based model, a first step towards calibration would be to record the plan dimensions of individual obstacles, such as an illegally parked car, a vendor's stall or a pile of bulky waste, and to map them onto the model grid at their surveyed positions, so that each object blocks the number of cells corresponding to its real footprint rather than a uniform cell. Combined with measured clear widths and pedestrian counts, this mapping would allow simulated speeds and flows to be compared with field observations and would give the model calibration and, eventually, predictive value.

In summary, the evidence favours a mixed strategy led by accessibility compliance, waste management and targeted structural repair, with enforcement and the management

of informal uses in support; its scope is limited by a single district, a single coder and a single survey period.

5. Conclusions

This study converted a micro-scale sidewalk audit of 52 street-unit sides nested within 26 street units in central Blida, Algeria, into a ranked set of municipal intervention families. Its main findings answer the three research questions as follows.

First, once counts are normalised per 100 m, the audit separates into two operational profiles: a stable lower-obstruction profile (31 sides) and a heterogeneous higher-obstruction profile (21 sides). Normative accessibility, bulky waste, and structural defects distinguish the profiles most strongly (27.3%, 22.6%, and 15.9% of attribution), with threshold-like effects at about 4–6 accessibility deficits, 1–1.6 bulky-waste items, and 2.5–3.5 structural defects per 100 m. Illegal parking, prominent in raw counts, becomes secondary after normalisation, and street furniture carries little weight. The SHAP ordering closely matches the simpler univariate ordering (Spearman $\rho = 0.98$). Normative accessibility leads under every robustness check, whereas the order of the second-tier families depends on the number of profiles; the ordering is an internal ranking that should be confirmed against independent evidence before it guides budget allocation.

Second, the minimal agent-based model shows that purely local avoidance can turn accumulated obstruction into a nonlinear loss of pedestrian performance, with systematic deterioration around 0.26–0.30 blocked-cell density and a steeper decline beyond 0.32. These values are specific to the dimensionless model and are not field thresholds for Blida.

Third, no single cause dominates obstruction in central Blida: accessibility deficits, waste, structural deficiencies, and informal uses all contribute. With accessibility deficits included, physical works (49.4%) and use regulation (45.4%) carry similar shares of attribution; when only physical occupation of the sidewalk is considered, use regulation leads (62.5%), driven by bulky-waste management and parking enforcement. Both readings support a mixed strategy: phased accessibility compliance, systematic waste collection, targeted structural repair, parking enforcement and negotiated management of commercial uses (Table 9).

Future research should pursue four directions: (i) a blind re-coding of the photographic record by a second coder to measure inter-rater reliability; (ii) normalisation by sidewalk area or effective clear width, and extension of the audit to other districts and cities; (iii) validation of the obstruction profiles and of the internal priority ranking against an independent outcome, such as observed pedestrian behaviour or expert ratings; and (iv) calibration of the agent-based model with measured sidewalk widths, obstacle footprints and pedestrian flows, followed by before-and-after evaluation of interventions. Within its present scope, the study provides a reproducible, low-data route from a detailed sidewalk audit to an interpretable hierarchy of intervention needs, and thereby supports municipalities in making sidewalks safer, more inclusive and more sustainable.

Supplementary Materials: The following supporting information can be downloaded at: https://www.mdpi.com/article/10.3390/su182111253/s1, File S1: Obstacles_Blida_densites_100m_Orange_v2.xlsx (audit data: raw counts, occurrences per 100 m and street-unit lengths for the 52 street-unit sides); File S2: Troncons_Blida.gpkg (digitised street-unit centrelines, WGS 84/UTM zone 31N); File S3: analyses_reviewers_Blida_v2.R (*k*-means partitioning, internal indices, gap statistic, street-unit bootstrap, random forest with grouped validation and TreeSHAP attribution); File S4: analyses_coherence_Blida_v2.R (descriptive statistics, principal component analysis, decision tree, hierarchical clustering, multidimensional scaling and silhouette analysis); File S5: robustness_checks_Blida.R (robustness of the family ordering, Appendix D); File S6: heure_passage_Blida.R (analysis of recorded visit times, Section 4.5).

Author Contributions: Conceptualization, L.R. and R.B.; methodology, L.R., R.B. and A.B.; software, L.R.; validation, R.B., A.B., S.K. and W.R.B.; formal analysis, L.R.; investigation, L.R.; resources, N.M.; data curation, L.R.; writing—original draft preparation, L.R.; writing—review and editing, R.B., A.B., S.K., N.M. and W.R.B.; visualization, L.R.; supervision, R.B. and A.B.; project administration, R.B. All authors have read and agreed to the published version of the manuscript.

Funding: This research received no external funding.

Institutional Review Board Statement: Not applicable.

Informed Consent Statement: Not applicable.

Data Availability Statement: The per-100 m audit data, the digitised street-unit geometries and the R scripts reproducing all analyses are provided as Supplementary Materials. Photographs are retained by the authors as internal documentation and are not distributed.

Acknowledgments: The authors thank the 25 third-year students of the Institute of Architecture and Urban Planning, University Saad Dahlab Blida 1, who carried out the field audit. During the preparation of this manuscript, the authors used the generative artificial-intelligence assistant Claude (Opus 5 and Opus 5.5; Anthropic) for language editing and for drafting R scripts that the authors ran and checked. The tool was not used to collect field data or to replace the authors' scientific judgement. All AI-assisted output was reviewed and verified by the authors, who take full responsibility for the content of the publication.

Conflicts of Interest: The authors declare no conflicts of interest.

Appendix A. Model Specification

This appendix consolidates the specification of the agent-based model introduced in Section 2.5.

Appendix A.1. Purpose and Status

The model tests whether a nonlinear relationship between blocked-cell density and pedestrian performance can emerge from purely local avoidance behaviour without imposing an aggregate density–throughput function. It is a mechanism-oriented exploratory model, not a predictive model of pedestrian flow in Blida and not a calibration of the sampled street geometry. Its supported claim is qualitative—nonlinear degradation can emerge under the stated rules—whereas the numerical location of the transition is model-specific.

Appendix A.2. Entities and Scales

Two entity types are represented. Patches form a rectangular lattice of $75 \times 6 = 450$ cells representing a sidewalk corridor running alongside a carriageway; each patch is either free or obstructed. Agents represent pedestrians and hold a position and a direction of travel toward the corridor exit; they have no memory, no route planning beyond the next cell, and no representation of other agents' intentions.

The lattice is dimensionless. One cell is a unit of occupancy rather than a calibrated area, so obstacle density is the proportion of the 450 cells that are obstructed, not a measurement in obstacles per square metre. One tick is one movement opportunity per agent; no real-time equivalent is claimed. Each run lasts 2000 ticks.

Appendix A.3. Process and Rules

At each tick, agents are injected at the entry row at a constant rate that does not saturate the corridor at density zero (Section 2.5); each active agent executes the movement rule below, and agents reaching the exit row are removed.

The movement rule is executed in three ordered attempts. First, the agent tries to advance one cell toward the exit. Failing that, it tries to step diagonally forward past

the blocking cell or agent. Failing that, it shuffles one cell sideways. If all three attempts fail, the agent remains in place, and a blocking event is recorded. A cell occupied by an obstacle or by another agent cannot be entered; this mutual exclusion is the only interaction between agents.

Obstacle positions are drawn at random at initialisation, subject to the density parameter, and remain fixed for the duration of a run. The density parameter was swept from 0 to 0.40 in steps of 0.02, with 20 independent replications at each level, giving 420 runs.

Appendix A.4. Outputs

Throughput is the number of agents crossing the exit boundary per tick, averaged over the run and normalised by the value obtained at density zero. Effective speed is the mean forward displacement per agent per tick, normalised in the same way. Blocking events are counted as described above. Mean crossing time was logged but is not used in the analysis, because at high density it is biased downward: only agents on the least obstructed paths ever complete the corridor.

Appendix A.5. Verification and Known Limits

At density zero, all agents traverse the corridor without blocking events, and that run defines the free-flow normalisation. Small excursions above 100% in Table 8 reflect replication noise at twenty replications per level. The flat low-density region depends partly on the sub-saturating injection regime, and the model is not mapped onto audit occurrence counts (Section 2.5). Accordingly, the transition region is a model-specific qualitative landmark rather than a metric standard or a field threshold.

Appendix B. Supervised Summarisation of the Partition

This appendix reports the confusion matrix of the random forest whose validation metrics are given in Table 7.

Random-Forest Reconstruction

Accuracy, ROC AUC, F1, and the Matthews correlation coefficient were examined under the three validation schemes described in Section 2.3 [77–79].

Table A1 gives the confusion matrix under grouped cross-validation. Under leave-one-street-unit-out, 45 of the 52 sides are reconstructed (C1: 28 of 31; C2: 17 of 21); five of the seven errors involve transitional sides identified by the silhouette analysis: four of the seven negative-silhouette C2 sides (R3_S3-D, R8_S1-D, R8_S3-D, R8_S3-G) and the lowest-silhouette C1 side (R3_S4-G).

Table A1. Confusion matrix of the random forest under five-fold cross-validation grouped by street unit (mean counts over 20 repetitions).

Observed/Predicted	Predicted C1	Predicted C2	Total
Observed C1	28.2	2.8	31
Observed C2	2.4	18.6	21
Total	30.6	21.4	52

Appendix C. Raw Counts and Occurrences per 100 m

Table A2 cross-tabulates the raw-count and per-100 m partitions compared in Section 3.2. Re-running *k*-means on raw counts gives the 34/18 partition reported in the original submission (silhouette 0.398 on standardised variables).

Table A2. Cross-tabulation of the raw-count and per-100 m two-profile partitions (52 street-unit sides).

Raw Counts/per 100 m	C1 (per 100 m)	C2 (per 100 m)	Total
C1 (raw counts)	24	10	34
C2 (raw counts)	7	11	18
Total	31	21	52

Appendix D. Robustness of the Family Ordering

Table A3 compares the internal ordering of the eight families under the two-profile and four-profile *k*-means solutions and reports its stability under grouped resampling. Both orderings use the random-forest and TreeSHAP settings of Table 6 (100 trees, maximum depth 15, minimum node size 5; seeds 0–99); the two-profile values reproduce Table 6 to within 0.1 percentage points. Because exact TreeSHAP for ranger forests is available for two-class models only, the four-profile ordering sums the mean absolute SHAP values of four one-versus-rest forests, one per profile. The grouped-resampling column refits the random forest within each training set of the five-fold cross-validation grouped by street unit (20 repetitions, 100 fits) and records how often each family ranks among the three leading families.

Under the four-profile solution, normative accessibility remains first, but street furniture and illegal parking rise to second and third place. The four profiles comprise a low-obstruction group (22 sides), an intermediate group (18 sides), a small group with high street-furniture and construction-site densities (5 sides), and a dense core (7 sides). Street furniture and construction sites therefore gain weight because they define the small group, not because they distinguish lower- from higher-obstruction sides. The rank correlation between the two orderings is 0.69, and the median rank correlation between each grouped-resampling fit and the full-sample ordering is 0.95 (range 0.67–1.00).

To assess the influence of survey timing, *k*-means was repeated on the five time-insensitive families only (structural defects, street furniture, normative accessibility, natural obstacles, and construction sites). This partition assigns 46 of the 52 street-unit sides (88%) to the same profile as the main partition (adjusted Rand index = 0.58), and within it normative accessibility (47.3%) and structural defects (26.5%) remain the leading families, ahead of street furniture (12.3%), natural obstacles (8.7%), and construction sites (5.2%).

Table A3. Mean absolute SHAP attribution (%) of the eight obstacle families under the two-profile and four-profile solutions (rank in brackets), and percentage of grouped-resampling fits in which each family ranks among the three leading families.

Obstacle Family	Two Profiles, $k = 2$	Four Profiles, $k = 4$	Top Three, Grouped Folds (%)
X3 Normative accessibility	27.3 (1)	21.5 (1)	100
X6 Bulky waste	22.6 (2)	11.2 (4)	99
X1 Structural defects	15.8 (3)	10.4 (6)	65
X5 Illegal parking	14.9 (4)	16.0 (3)	34
X2 Street furniture	6.3 (5)	18.7 (2)	0
X4 Commercial occupation	5.4 (6)	10.7 (5)	0
X7 Natural obstacles	5.1 (7)	4.4 (8)	2
X8 Construction sites	2.6 (8)	7.1 (7)	0

References

1. Lawson, A.; Lynch, D.; Orchard, M.; Raseta, S.; Standing, W. Fostering awareness of what stops pedestrian environments being inclusive and accessible: Resources and reflections from a multinational study. *Proj. Repos. J.* **2025**, *23*, 98–101. [CrossRef]
2. Nahdatunnisa, N.; Tahir, M.A.; Fajar, F. Aksesibilitas Jalur Pedestrian Menuju Kota Inklusif dan Berkelanjutan [Pedestrian path accessibility towards an inclusive and sustainable city]. *J. Rekayasa Sipil Dan Lingkung.* **2024**, *8*, 146–157. (In Indonesian) [CrossRef]

3. Sheller, M. *Mobility Justice: The Politics of Movement in an Age of Extremes*; Verso: London, UK, 2018.
4. Southworth, M. Designing the walkable city. *J. Urban Plan. Dev.* **2005**, *131*, 246–257. [CrossRef]
5. Bartzokas-Tsiompras, A.; Bakogiannis, E.; Nikitas, A. Global microscale walkability ratings and rankings: A novel composite indicator for 59 European city centres. *J. Transp. Geogr.* **2023**, *111*, 103645. [CrossRef]
6. Bivina, G.R.; Gupta, A.; Parida, M. Influence of microscale environmental factors on perceived walk accessibility to metro stations. *Transp. Res. Part D Transp. Environ.* **2019**, *67*, 142–155. [CrossRef]
7. Ewing, R.; Cervero, R. Travel and the built environment: A meta-analysis. *J. Am. Plan. Assoc.* **2010**, *76*, 265–294. [CrossRef]
8. Ewing, R.; Handy, S. Measuring the unmeasurable: Urban design qualities related to walkability. *J. Urban Des.* **2009**, *14*, 65–84. [CrossRef]
9. Saelens, B.E.; Handy, S.L. Built environment correlates of walking: A review. *Med. Sci. Sports Exerc.* **2008**, *40*, S550–S566. [CrossRef] [PubMed]
10. De Vos, J.; Lättman, K.; van der Vlugt, A.-L.; Welsch, J.; Otsuka, N. Determinants and effects of perceived walkability: A literature review, conceptual model and research agenda. *Transp. Rev.* **2022**, *43*, 303–324. [CrossRef]
11. Kim, B.; Barrington, W.E.; Dobra, A.; Rosenberg, D.; Hurvitz, P.; Belza, B. Mediating role of walking between perceived and objective walkability and cognitive function in older adults. *Health Place* **2023**, *79*, 102943. [CrossRef] [PubMed]
12. Vichiensan, V.; Nakamura, K. Walkability perception in Asian cities: A comparative study in Bangkok and Nagoya. *Sustainability* **2021**, *13*, 6825. [CrossRef]
13. Banister, D. The sustainable mobility paradigm. *Transp. Policy* **2008**, *15*, 73–80. [CrossRef]
14. Mei, Y.; Wang, S.; Gong, M.; Chen, J. Urban traffic dominance: A dynamic assessment using multi-source data in Shanghai. *Sustainability* **2024**, *16*, 4956. [CrossRef]
15. Anjaria, J.S. Street hawkers and public space in Mumbai. *Econ. Political Wkly.* **2006**, *41*, 2140–2146.
16. Bromley, R. Street vending and public policy: A global review. *Int. J. Sociol. Soc. Policy* **2000**, *20*, 1–28. [CrossRef]
17. Jacobs, J. *The Death and Life of Great American Cities*; Random House: New York, NY, USA, 1961.
18. Kim, A.M. *Sidewalk City: Remapping Public Space in Ho Chi Minh City*; University of Chicago Press: Chicago, IL, USA, 2015.
19. Oranratmanee, R.; Sachakul, V. Streets as public spaces in Southeast Asia: Case studies of Thai pedestrian streets. *J. Urban Des.* **2014**, *19*, 211–229. [CrossRef]
20. Peimani, N.; Kamalipour, H. Informal street vending: A systematic review. *Land* **2022**, *11*, 829. [CrossRef]
21. Boonjubun, C. Conflicts over streets: The eviction of Bangkok street vendors. *Cities* **2017**, *70*, 22–31. [CrossRef]
22. Eidse, N.; Turner, S.; Oswin, N. Contesting street spaces in a socialist city: Itinerant vending-scapes and the everyday politics of mobility in Hanoi, Vietnam. *Ann. Am. Assoc. Geogr.* **2016**, *106*, 340–349. [CrossRef]
23. Jacob, A.A. Influence of urban street vending on pedestrian experience and behaviour: A systematic quantitative review. *J. Contemp. Urban Aff.* **2023**, *7*, 139–163. [CrossRef]
24. Arellana, J.; Alvarez, V.; Oviedo, D.; Guzman, L.A. Walk this way: Pedestrian accessibility and equity in Barranquilla and Soledad, Colombia. *Res. Transp. Econ.* **2021**, *86*, 101024. [CrossRef]
25. Friesen, J.; Georganos, S.; Haas, J. Differences in walking access to healthcare facilities between formal and informal areas in 19 sub-Saharan African cities. *Commun. Med.* **2025**, *5*, 47. [CrossRef] [PubMed]
26. Guevara-Quinchúa, Y.; Francel-Delgado, A.E. Walk and connect: Measurement of inclusion criteria for people with functional diversity. Ibagué, Colombia. *Heliyon* **2023**, *9*, e20987. [CrossRef] [PubMed]
27. Lucas, K. Transport and social exclusion: Where are we now? *Transp. Policy* **2012**, *20*, 105–113. [CrossRef]
28. Dados, N.; Connell, R. The Global South. *Contexts* **2012**, *11*, 12–13. [CrossRef]
29. Lévy, C. Urban development in the Global South. In *The Essential Guide to Critical Development Studies*; Routledge: London, UK, 2017; pp. 328–337. [CrossRef]
30. Parnell, S.; Robinson, J. (Re)theorizing cities from the Global South: Looking beyond neoliberalism. *Urban Geogr.* **2012**, *33*, 593–617. [CrossRef]
31. Robinson, J. *Ordinary Cities: Between Modernity and Development*; Routledge: London, UK, 2006. [CrossRef]
32. Simone, A. *City Life from Jakarta to Dakar: Movements at the Crossroads*; Routledge: New York, NY, USA, 2010.
33. Watson, V. Seeing from the South: Refocusing urban planning on the globe's central urban issues. *Urban Stud.* **2009**, *46*, 2259–2275. [CrossRef]
34. Boudreau, J.-A.; Davis, D.E. Introduction: A processual approach to informalization. *Curr. Sociol.* **2017**, *65*, 151–166. [CrossRef]
35. Caldeira, T.P.R. Peripheral urbanization: Autoconstruction, transversal logics, and politics in cities of the global south. *Environ. Plan. D Soc. Space* **2017**, *35*, 3–20. [CrossRef]
36. Roy, A. Why India cannot plan its cities: Informality, insurgence and the idiom of urbanization. *Plan. Theory* **2009**, *8*, 76–87. [CrossRef]
37. Shaaban, K. Assessing sidewalk and corridor walkability in developing countries. *Sustainability* **2019**, *11*, 3865. [CrossRef]

38. Eldeeb, S.; Masoumi, H. Investigating walkability and bikeability in compact vs. new extensions: The case of Greater Cairo. *Front. Built Environ.* **2023**, *9*, 1165996. [CrossRef]
39. Cobbinah, P.B.; Finn, B.M. On pedestrian accessibility: Spatial justice and progressive planning in African cities. *J. Plan. Lit.* **2025**, *40*, 170–184. [CrossRef]
40. Okyere, S.A.; Frimpong, L.K.; Boateng, F.G.; Mensah, S.L.; Oviedo, D.; Abunyewah, M.; Kita, M. Walking cities that are (un)walkable: Exploring everyday lived realities in low-income neighbourhoods in Accra. *Transportation* **2026**, *53*, 459–482. [CrossRef]
41. Gebremariam, D.; Kuhilen, T.; Seboka, H.; Grum, B. Effect of sidewalk design and obstructions on pedestrian mobility: A case study of the main streets of Mekelle City, Northern Ethiopia. *Adv. Civ. Eng.* **2024**, *2024*, 5672280. [CrossRef]
42. Aghaabbasi, M.; Moeinaddini, M.; Zaly Shah, M.; Asadi-Shekari, Z.; Arjomand Kermani, M. Evaluating the capability of walkability audit tools for assessing sidewalks. *Sustain. Cities Soc.* **2018**, *37*, 475–484. [CrossRef]
43. Arellana, J.; Saltarín, M.; Larrañaga, A.M.; Alvarez, V.; Henao, C.A. Urban walkability considering pedestrians' perceptions of the built environment: A 10-year review and a case study in a medium-sized city in Latin America. *Transp. Rev.* **2020**, *40*, 183–203. [CrossRef]
44. Venerandi, A.; Mellen, H.; Romice, O.; Porta, S. Walkability indices—The state of the art and future directions: A systematic review. *Sustainability* **2024**, *16*, 6730. [CrossRef]
45. Koo, B.W.; Guhathakurta, S.; Botchwey, N. Development and validation of automated microscale walkability audit method. *Health Place* **2022**, *73*, 102733. [CrossRef] [PubMed]
46. Liu, L.; Wang, H.; Wu, C. A machine learning method for the large-scale evaluation of urban visual environment. *arXiv* **2016**, arXiv:1608.03396. [CrossRef]
47. Wang, J.; Biljecki, F. Unsupervised machine learning in urban studies: A systematic review of applications. *Cities* **2022**, *129*, 103925. [CrossRef]
48. Ye, Y.; Zeng, W.; Shen, Q.; Zhang, X.; Lu, Y. The visual quality of streets: A human-centred continuous measurement based on machine learning algorithms and street view images. *Environ. Plan. B Urban Anal. City Sci.* **2019**, *46*, 1439–1457. [CrossRef]
49. Zünd, D.; Bettencourt, L.M.A. Street view imaging for automated assessments of urban infrastructure and services. In *Urban Informatics and Future Cities*; Springer: Singapore, 2021; pp. 29–40. [CrossRef]
50. United Nations. *Transforming Our World: The 2030 Agenda for Sustainable Development*; Resolution A/RES/70/1; United Nations General Assembly: New York, NY, USA, 2015.
51. People's Democratic Republic of Algeria. *Law No. 02-09 of 8 May 2002 on the Protection and Promotion of Persons with Disabilities*; No. 34; Official Gazette of the People's Democratic Republic of Algeria: Algiers, Algeria, 2002.
52. R Core Team. *R: A Language and Environment for Statistical Computing, Version 4.6.1*; R Foundation for Statistical Computing: Vienna, Austria, 2026; Available online: https://www.R-project.org/ (accessed on 22 August 2026).
53. Tibshirani, R.; Walther, G.; Hastie, T. Estimating the number of clusters in a data set via the gap statistic. *J. R. Stat. Soc. Ser. B Stat. Methodol.* **2001**, *63*, 411–423. [CrossRef]
54. Hennig, C. Cluster-wise assessment of cluster stability. *Comput. Stat. Data Anal.* **2007**, *52*, 258–271. [CrossRef]
55. Lundberg, S.M.; Erion, G.; Chen, H.; DeGrave, A.; Prutkin, J.M.; Nair, B.; Katz, R.; Himmelfarb, J.; Bansal, N.; Lee, S.-I. From local explanations to global understanding with explainable AI for trees. *Nat. Mach. Intell.* **2020**, *2*, 56–67. [CrossRef] [PubMed]
56. Meyer, H.; Pebesma, E. Machine learning-based global maps of ecological variables and the challenge of assessing them. *Nat. Commun.* **2022**, *13*, 2208. [CrossRef] [PubMed]
57. Hastie, T.; Tibshirani, R.; Friedman, J. *The Elements of Statistical Learning: Data Mining, Inference, and Prediction*, 2nd ed.; Springer: New York, NY, USA, 2009. [CrossRef]
58. Bonabeau, E. Agent-based modeling: Methods and techniques for simulating human systems. *Proc. Natl. Acad. Sci. USA* **2002**, *99*, 7280–7287. [CrossRef] [PubMed]
59. Hu, C.; Zhang, J.; Ren, W.; Liang, H. Simulation and optimization of pedestrian environments in urban residential neighborhoods based on agent-based modeling. *Front. Archit. Res.* **2026**. [CrossRef]
60. Blue, V.J.; Adler, J.L. Cellular automata microsimulation for modeling bi-directional pedestrian walkways. *Transp. Res. Part B Methodol.* **2001**, *35*, 293–312. [CrossRef]
61. Burstedde, C.; Klauck, K.; Schadschneider, A.; Zittartz, J. Simulation of pedestrian dynamics using a two-dimensional cellular automaton. *Phys. A* **2001**, *295*, 507–525. [CrossRef]
62. Helbing, D.; Molnár, P. Social force model for pedestrian dynamics. *Phys. Rev. E* **1995**, *51*, 4282–4286. [CrossRef] [PubMed]
63. Caprón, G.; Monnet, J.; Pérez López, R. The sidewalk: Between traffic and other uses, the challenges of a hybrid urban order. *Culturales* **2023**, *11*, e763. [CrossRef]
64. Sennett, R. *Building and Dwelling: Ethics for the City*; Allen Lane: London, UK, 2018.
65. Doan, Q.C.; Ma, J.; Chen, S.; Zhang, X. Nonlinear and threshold effects of the built environment, road vehicles and air pollution on urban vitality. *Landsc. Urban Plan.* **2025**, *253*, 105204. [CrossRef]

66. Li, C.; Zhou, Y.; Wu, M.; Xu, J.; Fu, X. Exploring nonlinear threshold effects and interactions between built environment and urban vitality at the block level using machine learning. *Land* **2025**, *14*, 1232. [CrossRef]
67. Yang, W.; Fei, J.; Li, Y.; Chen, H.; Liu, Y. Unraveling nonlinear and interaction effects of multilevel built environment features on outdoor jogging with explainable machine learning. *Cities* **2024**, *147*, 104813. [CrossRef]
68. Forde, A.; Daniel, J. Pedestrian walking speed at un-signalized midblock crosswalk and its impact on urban street segment performance. *J. Traffic Transp. Eng. (Engl. Ed.)* **2021**, *8*, 57–69. [CrossRef]
69. Moussaïd, M.; Helbing, D.; Theraulaz, G. How simple rules determine pedestrian behavior and crowd disasters. *Proc. Natl. Acad. Sci. USA* **2011**, *108*, 6884–6888. [CrossRef] [PubMed]
70. United Nations. *Convention on the Rights of Persons with Disabilities*; United Nations: New York, NY, USA, 2006.
71. Dovey, K.; Recio, R.B.; Pafka, E. The spatial logic of informal street vending in Manila: An assemblage approach. *Space Polity* **2022**, *26*, 192–215. [CrossRef]
72. Roy, A. Urban informality: Toward an epistemology of planning. *J. Am. Plan. Assoc.* **2005**, *71*, 147–158. [CrossRef]
73. Loukaitou-Sideris, A.; Ehrenfeucht, R. *Sidewalks: Conflict and Negotiation over Public Space*; MIT Press: Cambridge, MA, USA, 2009. [CrossRef]
74. Qazimirsaeed, A.; Khosravi, H.; Rafieian, M.; Mirzahossein, H.; Forciniti, C. Walkability policies in developing countries: What do people need and prefer in Iran? *Sustainability* **2022**, *14*, 10808. [CrossRef]
75. Prieto-Curiel, R.; Patino, J.E.; Anderson, B. Scaling of the morphology of African cities. *Proc. Natl. Acad. Sci. USA* **2023**, *120*, e2214254120. [CrossRef] [PubMed]
76. Datta, A. The digital turn in postcolonial urbanism: Smart citizenship in the making of India's 100 smart cities. *Trans. Inst. Br. Geogr.* **2018**, *43*, 405–419. [CrossRef]
77. Chicco, D.; Jurman, G. The advantages of the Matthews correlation coefficient (MCC) over F1 score and accuracy in binary classification evaluation. *BMC Genom.* **2020**, *21*, 6. [CrossRef] [PubMed]
78. Gorodkin, J. Comparing two K-category assignments by a K-category correlation coefficient. *Comput. Biol. Chem.* **2004**, *28*, 367–374. [CrossRef] [PubMed]
79. Farhadpour, S.; Warner, T.A.; Maxwell, A.E. Selecting and interpreting multiclass loss and accuracy assessment metrics for classifications with class imbalance: Guidance and best practices. *Remote Sens.* **2024**, *16*, 533. [CrossRef]

Disclaimer/Publisher's Note: The statements, opinions and data contained in all publications are solely those of the individual author(s) and contributor(s) and not of MDPI and/or the editor(s). MDPI and/or the editor(s) disclaim responsibility for any injury to people or property resulting from any ideas, methods, instructions or products referred to in the content.